A Review of Discontinuities (and Alfvén Waves) in Interplanetary Space: Ulysses Results

Bruce T. Tsurutani and Christian M. Ho
Jet Propulsion Laboratory
California Institute of Technology, Pasadena

Abstract

The Ulysses mission explored for the first time our heliosphere at all latitudes up to ± 80 and therefore has been an ideal mission to study potential gradients in heliolatitude (and radial distance) of discontinuity occurrence rates and types. Directional discontinuities (DDs) are shown to be dependent on the type of solar wind streams that they are embedded in. There are 5 to 10 times as many DDs in high-speed streams as in slow speed streams. The explanation is that rotational discontinuities (RDs) are the phase-steepened edges of Alfvén waves. The nonlinear Alfvén waves in high-speed streams have $\Delta\tilde{B}/B_o \sim 1-2$, and are arc-polarized spherical waves. Dissipation at these "intermediate shocks" (the RDs) have been sought, but not found. An $e^{-(R-1)/5}$ decrease in discontinuity rate with increasing radial distance (R) is partially an artifact of the selection criteria (discontinuity thickening), but dissipation at a relatively slow rate is also a possible contributor. There is no obvious latitudinal gradient in discontinuity types or occurrence rates. Somewhat surprisingly, TDs are detected at high latitudes. These have been associated with the edge of mirror mode structures and interfaces in the gradients of microstreams. A pair of slow shocks were detected at 5.3 AU. The speeds are similar to fast mode shock speeds. When Alfvén waves in high-speed streams impinge upon the Earth's magnetosphere, near continuous occurring substorms (called HILDCAAs) occur, leading to the pumping of an extraordinary amount of energy into the nightside ionosphere. Current discontinuity and Alfvén wave research problems are discussed.

INTRODUCTION

One of the fundamental microstructures present in the solar wind are directional discontinuities (DDs): sharp angular changes in the interplanetary magnetic field directionality (Burlaga, 1971). Theoretically, there can be several different types: rotational(RDs), tangential (TDs), shocks (fast, intermediate and slow), and contact discontinuities (CDs). CDs are not of particular interest for space plasmas, and therefore will not be covered here. The purpose of this paper is to discuss the new discontinuity results obtained from the Ulysses magnetic field and plasma data sets in context with previous results. In this review, RDs, TDs and slow shocks, will be covered. Fast shocks is a very broad topic and would be best left for a separate review article.

Figure 1 gives the properties of the four types of discontinuities, as discussed in Landau and Lifschitz (1960). This Figure illustrates the properties that can be used to distinguish the various types of discontinuities from one another. Tangential discontinuities have no mass flux flow across their surface. TDs can be thought of as a surface separating two different types of plasmas and is ideally infinite in extent. The field direction and magnitude can be different on the two sides as well as plasma densities, temperatures and even composition (H^+, He^{++}, $O^{+6/+7}$). TDs can be identified by the lack of a magnetic field normal ($H_n = 0$) across their surface. RDs have mass flow across their surfaces, nonzero magnetic field normal components, and for isotropic plasmas (however, see Hudson, 1964), the transverse component of H is constant ($[H_T] = 0$). RDs ideally have large field normal components and no changes in magnetic field magnitude. Shocks have mass flow across their surfaces, and neither the magnetic field normal component nor the transverse component need be conserved.

DD Radial and Latitudinal Gradients

The topics of radial and latitudinal gradients of DDs are important towards understanding their generation mechanisms and their evolution. For example, if TDs are dissipated/broadened through magnetic reconnection, or if RDs are dissipated through coupling to other electromagnetic or electrostatic modes (which are then in turn damped), these processes could have profound effects on the evolution of the solar wind plasma, and hence the heliosphere. TDs are thought to separate dissimilar plasmas and can be interplanetary markers of structures convected from the sun or its corona. RDs and Alfvén waves contribute to the scattering of solar energetic particles and cosmic rays.

There has been a controversy about the gradients in occurrence rate of DDs (Burlaga, 1971; Mariani et al., 1973; Behannon, 1978; Tsurutani and Smith, 1979; Lepping and Behannon, 1986). Much of the problem (and dispute) come from the difficulty in separating latitudinal effects from radial distance effects. The Ulysses spacecraft, which first went from 1 AU to 5 AU, and with a Jupiter gravity assist, to −80° latitude and finally to +80° latitude, was ideal to address this problem. Ulysses provided a full coverage of heliographic latitudes, and as we shall see, will allow a resolution to this problem.

There are two computerized methods of detecting DDs, one by Tsurutani and Smith (1979) hereafter called TS and another by Lepping and Behannon (1986) hereafter called LB. For large statistical studies it is necessary to identify DDs by computer analyses, as tens of thousands of discontinuities are often used (however, for determination of discontinuity type, no one has been able to automatic this yet). The TS criteria require a field directional change of $\Delta\vec{B}/|B| \geq 0.5$ and $|\Delta B|$ greater than 2σ when σ^2 is the variance on either side of the discontinuity. These criteria are applied to 1-min vectors when the two 1-min vectors being intercompared were separated by 3-min. This vector separation allows for discontinuities with "thicknesses" as large as 60s to be detected without bias. The LB criteria (slightly modified from the original method) require that field directional change between vectors be at least 30°, or $\theta = \cos^{-1}(\vec{B}_1 \cdot \vec{B}_2)/|B_1||B_2| \geq 30°$. $\vec{B}_1$ and $\vec{B}_2$ are by standard convention, the upstream and downstream field vectors. These criteria were applied to 1-min averages with $\vec{B}_1$ and $\vec{B}_2$ separated by 2 min. For more details concerning the methods of selection, we refer the reader to the original articles.

TDs and RDs are schematically shown in Figure 2. As mentioned before, TDs can be thought of as infinite sheets separating dissimilar plasmas and fields. RDs can be thought of as sharply kinked Alfvén waves, a topic which we will come back to later.

Figure 3, from Tsurutani et al. (1996a) shows the radial gradient of DD occurrence rate from 1 to 5 AU. Ulysses was in the ecliptic plane. The vertical scale is the normalized number of discontinuities per day, using 0.2 AU internal bins (the normalization takes data gaps into account). The TS and LB rate of interplanetary discontinuities (ROID) values are different (because of the slightly different criteria), but show the same general trend. Both plots show a gradual decrease in rate of occurrence with increasing radial distance. Both plots have been fitted by exponential curves. TS is best fit with $e^{-(r-1)/5}$ dependence where r is measured in AU. LB is best fit by a $e^{-(r-1)/4}$ dependence. This result is a confirmation of previous radial gradient

results of TS and LB, and has been explained partially as an effect of increasing discontinuity thickness with decreasing magnetic field strength (with increasing radial distance from the Sun). Some of the "thickened" discontinuities therefore fall outside the computerized selection criteria. Some part of this ROID decrease might also be due to the potential dissipation of discontinuities. A new criterion based on the orientation of the discontinuity, speed of the solar wind and magnetic field strength is needed to make further progress on this topic of potential dissipation.

The TS and LB ROID values are given in Figure 4 as Ulysses goes from the ecliptic plane to −80° latitude. The proton densities, temperatures and solar wind velocities are shown in the top three panels. Next is the interplanetary magnetic field (IMF) |B|, TS and LB ROID values, and lastly the Ulysses position in radial distance and heliolatitude. The spacecraft moves closer to the sun as it goes toward the pole (one can observe some radial dependence in the TS and LB ROID plots).

An important point to note in this figure is that the ROID value depends strongly on the type of stream structure that Ulysses encounters. From July 1992 through April 1993, there are recurring high-speed streams (Phillips et al., 1994) associated with a coronal hole that is centered at the south pole of the sun. The TS and LB ROID values increase and decrease in coincidence with the speed of the solar wind. A typical ratio of the ROID value in a high-speed stream to that outside the stream is ~5:1 to 10:1.

After August 1993, Ulysses was permanently embedded in a high-speed stream with V_{sw} = 700-800 km s^{-1}. The TS ROID value remained between 80 and 100 discontinuities day^{-1}. Thus there is a stream dependence on the ROID values which overrides any latitudinal gradient that may be present. We will focus on this first-order dependence.

Alfvén Waves and Discontinuities

In parallel with the discontinuity work, it was found that the high-speed wind was characterized by the presence of large-amplitude nonlinear Alfvén waves (Tsurutani et al., 1994; Smith et al., 1995; Balogh et al., 1995). Such a dependence could have been inferred from in-ecliptic date a long time ago (Belcher and Davis, 1971), but stream-stream interactions tended to cloud the issue. Figure 5 illustrates these fluctuations in the three velocity and three magnetic field components. The dates were taken when Ulysses was 2.8 AU from the sun at a heliolatitude of −70°. The data are presented in the RTN coordinate system, where $\hat{R}$ is radially outward from

the sun, $\hat{T}$ is defined by $(\hat{\Omega}x\hat{R})/|\hat{\Omega}x\hat{R}|$, where $\hat{\Omega}$ is the solar rotation axis. $\hat{N}$ completes the right-hand system. Note that the scale for V_R is different than the other two components of velocity. Ignoring the large-amplitude, slow ~3-day variations in V_R and concentrating on the higher frequency components, we note that $|\Delta\vec{B}|/|B|$ is typically ~1 to 2, indicating that these waves are highly nonlinear.

Belcher and Davis (1971) used $\vec{V}-\vec{B}$ cross correlation analyses to identify Alfvénic fluctuations in the interplanetary medium, and noted that the sign of the correlation coefficient determines the direction of wave propagation. Figure 6 are the cross-correlation results of the R, T and N components of $\vec{V}$ and $\vec{B}$ of Figure 5. We note a peak correlation coefficient at zero lag with values of 0.64, 0.86 and 0.85, respectively. Thus these waves appear to be highly Alfvénic and are propagating outward from the sun. Such high correlation values for the transverse components (T and N) are unusual for such long time intervals (24 hr). Analyses of in-ecliptic plasma usually are done over 6 to 12 hrs (to illustrate Alfvénicity). If the polar coronal hole Alfvén waves are intrinsically the same as coronal hole waves near the ecliptic plane, the lack of pure Alfvénicity of waves detected near the Earth imply that either stream-stream interactions or the wrapping up of the IMF must be important for the development of turbulence.

To compare wave properties near the center of the polar coronal hole to those near the edge, we select seven (7) intervals of two days each. Each interval was selected to be within the trailing portion of a high-speed stream to avoid stream-stream interaction regions. Alfvén waves were present. The intervals are shown in Table 1. We have shown the average solar wind speed, density, proton temperature, radial distance and heliographic latitude for each interval as well.

Power spectra were calculated for each of the intervals. These spectra were normalized by dividing by the average magnetic field magnitude squared. This was done to be able to intercompare values at different radial distances when the field strengths were significantly different. The normalized power, or B_n^2/B_o^2, is also a more fundamental parameter in physical terms. It can be used to calculate resonant pitch angle scattering by transverse waves (Kennel and Petschek, 1966; Tsurutani and Lakhina, 1997c).

Although all seven intervals were analyzed, for brevity, we illustrate only two in Figure 7, the results for days 20-21, 1991 near the ecliptic plane (−2° latitude) and days 238-239, 1994 near the south pole (−79° latitude), are shown. The normalized power spectra for these two - 2 day intervals are shown in the top row of the Figure.

The normalized transverse power spectra and the normalized magnetic field magnitude power spectra were calculated and are given as the top left two panels. To determine the "transverse power" spectra, we first determine the average field direction over the interval, transform the magnetic field into this coordinate system and then calculate the power in the two orthogonal components. The "transverse power" is the average of the power in these two components. The value obtained will be a lower limit, especially if the ambient field had significant directional variations during the two days. Possible variations can be checked either by simple visual inspection or by comparison of the magnitude of the transverse power to the power in the field-aligned component. In comparing the latter, we note that the power in the transverse component was considerably greater than that of the field-aligned component (not shown), indicating that the directional variations was not a major problem.

In examining the results in the top four panels of Figure 7, we note that the spectral shape over the frequency range of 10^{-4} to 10^{-1} Hz is $f^{-1.6}$ to $f^{-1.7}$, independent of latitude or whether one is examining the transverse component or the field magnitude component. The normalized transverse wave power over the pole is a factor of ~2 times that in the ecliptic ($2 \times 10^{-4}\ f^{-1.7}$ compared to $1.0 \times 10^{-4}\ f^{-1.6}$). The same is true for the normalized field magnitude wave power. The comparative numbers are $2.4 \times 10^{-5}\ f^{-1.6}$ to $1.1 \times 10^{-5}\ f^{-1.6}$, respectively. The power in the field magnitude is lower than the transverse component by a factor of ~10.

The normalized wave power over ten-day intervals have also been examined. The results are given in the bottom four panels of Figure 7. The intervals of study are days 20-30, 1991 and days 230-240, 1994. Since these intervals cover the two 2-day intervals just discussed, an intercomparison can be made.

Figure 7b shows the normalized wave power between ~10^{-5} to 10^{-2} Hz. The transverse wave power for the 10-day interval at high heliolatitudes ($2.5 \times 10^{-4}\ f^{-1.6}$) is essentially the same as for the 2-day interval ($2.0 \times 10^{-4}\ f^{-1.7}$). This is what one would expect from a region of continuous high-stream flow with embedded Alfvén waves. However, the results are different for the near-ecliptic power spectra. The transverse power for the 10-day interval ($4.0 \times 10^{-5}\ f^{-1.5}$) is considerably less than for the 2-day interval ($1.0 \times 10^{-4}\ f^{-1.6}$). There are several possible explanations. Wave events in the ecliptic plane often only last a few days and not 10 days. Thus the spectra could be taken over a "pure" mix of Alfvén wave events plus more quiet solar wind conditions. A second possibility is that longer intervals will encompass more field directional

variations and the "average" direction will be less well defined. A third possibility is there is a boundary region (near the sun) separating fast and slow streams and this region is intermediate in Alfvénicity. Most probably several of these factors contribute to these spectral differences. There is about the same amount of compressional wave power in the 10-day interval (6.9×10^{-6} $f^{-1.5}$) as in the 2-day interval ($1.1\ 10^{-5}\ f^{-1.6}$).

Discontinuity "Thicknesses"

The greater number of discontinuities in high-speed flows can be related to either some intrinsic relationship between Alfvén waves and discontinuities or to the fast convective flow of discontinuities past the spacecraft. For the latter case, a faster flow means that thicker discontinuities will be picked up by the computer selection criteria, and more of the discontinuity thickness "distribution" will be detected. To explore this latter effect first, we examine discontinuity thicknesses.

Figure 8 gives the discontinuity "temporal" thicknesses for discontinuities at −67° latitude at 3.0 AU. This is the day 154-155, 1994 interval of Table 1. We use "temporal" thickness rather than spatial values because it is the "temporal" thickness distributions that is the issue here for the computer selection criteria. Each discontinuity thickness was determined by hand-analysis of high resolution magnetic field data. The 2/e (65%) value of the total angular change was determined to define the temporal thickness. The temporal thickness distribution for all of the TS discontinuities detected during the 2-day interval is given in panel 7a.

The discontinuity spatial thicknesses can be determined by performing minimum variance analyses to determine the minimum variance direction (or normal direction) and calculating the thickness by the expression $V_{SW}\ \Delta T \cos\theta_{nV}$ where V_{SW} is the solar wind speed, ΔT the temporal thickness, and θ_{nV} the angle between the discontinuity normal and the solar wind velocity vector. For simplicity of calculation, we assume that the solar wind velocity lies along the $-\hat{R}$ direction (in reality the velocity may deviate a few degrees from this direction in polar coronal hole high-speed flows). Making this simplifying assumption only leads to minor errors. The spatial thickness distribution for days 154 to 155, 1994 are shown in Figure 8b.

In the above calculations, it was assumed that the discontinuities were simply convected by the solar wind. This is true if the discontinuities are TDs. On the other hand, if most of the events are RDs (we will argue this case later), then the discontinuity structures will be propagating

relative to the solar wind. The Alfvén speed varies from 40 to 70 km s^{-1}, whereas the solar wind varies from 400 to 800 km s^{-1}. Thus the RD propagation is only a ~10% correction factor, and to first order can be neglected. For our purposes, we can assume that both RDs and TDs are simply convected by the solar wind.

The distributions in Figure 8 indicate that most discontinuities are small scale features. There is a "tail" to the distribution but the number of discontinuities falls off with increasing thickness.

A simple calculation using the solar wind speeds and the top panel values, can be used to demonstrate that the increased solar wind speeds cannot be the total cause of the ROID value increase in high-speed streams. The solar wind speed during days 154 and 155 was a near-constant ~750 km s^{-1}. If the solar wind speed were lowered to slow speed values of ~400 km s^{-1}, then some of the thicker discontinuities would be missed. An upper bound on this number can be easily calculated in the following manner. The TS selection method detects all discontinuities with thicknesses less than 60s. Discontinuities with thicknesses between 60s and 120s can be detected without bias if their location is well placed (start and stop times) within the time interval. Discontinuities thicker than 120s can also be detected if their vector changes ($\Delta\vec{B}/|B|$) are sufficiently large (>0.5). Thus the cutoff on the 60s thickness discontinuities would be 400 km s^{-1}/750 km s^{-1} x 60s or 32s. All discontinuities with thicknesses less than 32s in Figure 8 would be detected in a 400 km s^{-1} solar wind stream. From Figure 8a, that would correspond to 89 on of the 171 discontinuities, or a ratio of ~2.0. Some of the thickness discontinuities would also be detected in a slower speed stream, so as previously mentioned, this is only an upper limit on the ROID value variability. Similar analyses have been done with LB discontinuities, and similar results were found.

The solar speed variations cannot account for the ROID value variations of ~5 to ~10. Thus, some other explanations must be found.

The Relationship Between Discontinuities and Alfvén Waves

Figure 9 illustrates one 24-hr period of the interplanetary magnetic field at high heliographic latitudes. This is day 17, 1992. Ulysses was in the elliptic plane (-6.0 latitude) 5.2 AU from the sun. The field is displayed in RTN coordinates. The TS selected discontinuities are identified by vertical lines. By visual inspection, one can note a relationship between slowly rotating fields

(Alfvén waves) and the sharp directional changes (DDs). Most of the DDs exhibits little or no magnetic magnitude changes, indicating that they are most likely rotational in nature.

Discontinuities often occur at the edge of slowly rotating fields. Figure 10 shows such an example. This interval occurs on day 210, 1995 when Ulysses was at +80.2° heliographic latitude. Other examples have been noted in the ecliptic plane and at midlatitudes. The results were essentially the same.

The magnetic field is plotted in minimum variance coordinates where B_1, B_2 and B_3 correspond to the field component along the maximum, intermediate and minimum variance directions. Point 1 at 2325:31 UT designates the start of a slow field rotation seen primarily in the B_1 component. Point 2 at ~2340:47 UT is the end of the slow rotation and the start of a faster field rotation interval. Point 3 is the end of the fast field rotation and interval of analysis. The top panel displays the field in minimum variance coordinates. The bottom panel is a hodogram of the B_1 - B_2 components. In the latter panel, the field rotates from left-to-right in an arc. From point 2 to 3, the field rotates back, completing the "arc" rotation. The field rotation is, to first order, noncompressive. The rotation occurs in a plane (not shown). Thus the discontinuity is believed to be part of the Alfvén wave, and thus we say that the Alfvén wave is "phase steepened", there is more phase rotation at one edge of the wave.

Riley et al. (1996) have shown that in the ecliptic plane, the arc-polarized waves account for 5 to 10% of the Ulysses data set. The waves are propagating outward in the rest frame of the solar wind plasma. An example of a 2 hr and 40 min sequence of waves on day 250, 1991 is shown as Figure 11. Here $B_{max} = B_1$, $B_{int} = B_2$.

A schematic illustrating the difference between planar waves and spherical waves (when the field magnitude is preserved) is shown in Figure 12. For planar waves (panel a), there are two fundamental polarizations, circular and elliptical (where linear polarization is a mix of equal amplitude left-and right-circular polarization) with left-handed and right-handed rotations. For large amplitude waves where the magnetic field is constant (panel b), there are circular and elliptic polarizations possible, and also an arc-polarization. The circular and arc-polarization perturbation vectors occur in a plane, while elliptically polarized waves are three-dimensional (not planar). Note that arc polarization is the large amplitude equivalent to the small amplitude linear case. Tsurutani et al. (1997b) have suggested that interplanetary waves are spherical arc-polarized structures.

Alfvénic Shocks?

Because noncompressional Alfvén waves have speeds intermediate between fast (magnetosonic) and slow (sound) waves in the solar wind, in MHD they are considered "intermediate" waves. The strong phase steepening indicates that dispersion and perhaps dissipation is occurring. To investigate the possibility that these discontinuities are Alfvénic (or intermediate) shocks, we examine the jump (upstream versus downsteam) conditions across the discontinuities.

Since the Alfvén waves in the polar regions above the sun are almost propagating purely outwards, this is an easy test for us to make. We simply assume all of the waves are propagated radially outward. Thus, in standard notation, the antisunward region is region 1 or the "upstream" region, and the sunward region is region 2, or the "downstream" region.

Figure 13 shows the relative jumps in density, temperature, magnetic field strength and velocity plotted against each other. In each case we use a standard rotation: ΔX is equal to $X_2 - X_1$ and X is X_1. Basically, we find the solar wind parameter jumps vary by ~10%, but not in any consistent fashion. The variations appear to be random. Thus we find no obvious dissipation effects in the statistical analyses.

The lack of a pattern to the jump conditions does not mean that these phase steepened Alfvén waves are not intermediate shocks. It simply implies that if there is dissipation, the process is much slower than the short interval of the measurements of the interplanetary parameters.

North-South Asymmetries?

One fundamental question concerning the heliosphere is: are there north-south asymmetries? This is related to cosmic ray particle transport, size of the polar coronal holes and magnetic fields in the two regions. To answer the question of possible asymmetries, all discontinuities within 1 month near the north polar pass (days 201-231, 1995, heliographic latitude +80°) were compared to one month near the south pole (days 226-256, 1994, heliograph latitude -80°). Figure 14 shows the TS ROID value plus other interplanetary parameters. It is noted that the plasma density, temperature, magnetic field magnitude and ROID value are slightly higher at the north pole compared to the south pole. However, the two polar passes occurred at slightly different radial distances, and this must be taken into account. At the north pole at 2.0 AU, the ROID value is 115 DDs/day. At the south pole at 2.3 AU, the ROID value was 105 DDs/day. If one normalizes the south polar data by the previously determined radial gradient of $e^{-(r-1)/5}$ AU, the

south pole value would be 113 DDs/day at 2.0 AU. Thus there is no obvious north-south asymmetry in ROID values.

Evolution of Nonlinear Alfvén Waves and Rotational Discontinuities

Medvedev et al. (1998) have studied the nonlinear dynamics of Alfvén wave trains in a $\beta \sim 1$, isothermal plasma, using the kinetic nonlinear Schroedinger (KNLS) model. They find that the combined effects of wave nonlinearity and Landau damping result in the stationary 'S" and arc-polarized rotational discontinuities. Buti et al. (1998a) analyzing Alfvén waves propagating in a medium with nonuniform densities and inhomogeneous magnetic fields, find that waves steepened and can be accelerated. The numerical solution, a form of a modified derivative nonlinear Schroedinger equation (MDLS) evolves into turbulence due to inhomogeneities.

Vasquez and Hollweg (1998a, b) have also attempted to explain the formation of arc- polarized rotational discontinuities associated with Alfvén waves. From a 2-1/2 D hybrid numerical simulations of oblique Alfvén waves with linear polarizations, it is found that the Alfvén waves evolve into spherical waves with arc-polarization. Vasquez and Hollweg (1998a) suggest that the RDs are steady with their normals oblique to $\vec{B}_0$. Vasquez and Hollweg (1998b), attempt to produce RDs with small normal angles to $\vec{B}_0$. To do this they start with linearly polarized waves with propagation angles $\leq 10^\circ$ to $\beta = 8\pi \sum_i N_i k T_i / |B|^2$. The waves, even for small amplitudes. tend to steepen and form RDs with normals nearly along $\vec{B}_0$. However the authors find that the RDs constantly widen due to dispersion effects. The authors conclude that Alfvén waves with embedded RDs "must evolve through a succession of arc-polarized or spherically polarized waveforms as they travel outward from the sun".

TDs versus RDs

From the previous discussion, because there is such a large increase in DD rates within high-speed streams, one would certainly expect all increases to be associated with an increases in occurrence of RDs. Also since there are no major streams present (but there are "microstreams": Neugebauer et al., 1995), there should not be many TDs found associated with stream-stream interactions. During the 1994-1995 period of solar minimum, the heliospheric current sheet was in the ecliptic plane, and there also should not be TDs associated with neutral sheets at high heliographic latitudes as well (Smith et al., 1993).

To identify the discontinuity type, we follow the Smith (1973 a,b) method of using discontinuity "phase space" regions. The minimum variance method is again used to rotate the IMF into this system to determine B_3, the normal to the discontinuity. We divide by the larger field magnitude on either side of the discontinuity and also measure the field magnitude jump across the structure. The particular "phase space" we use is B_3/B_L and $\Delta|\bar{B}|/B_L$ where $\Delta|\bar{B}|$ is the magnitude of the field vector change across the discontinuity and B_L is the larger field magnitude on either side of the discontinuity.

For 4 days where Ulysses was over the north heliographic pole (days 218-221, 1995), all 416 discontinuities that were selected by the TS criteria were analyzed. These are displayed in discontinuity phase space as Figure 15. Events with large $\Delta|B|/B_L$ and small B_3/B_L are identified as TDs. The cutoff for this type of discontinuity is arbitrary, but we use $\Delta|B|/B_L > 0.2$ and $B_3/B_L < 0.2$. The number of clear TDs is 6.1% of the total.

Ho et al. (1995) examined the 1486 discontinuities identified during 15 days near the south pole. They identify 78 clear TDs or an occurrence rate of 5.2% relative to all DDs. This number is also quite close to values taken in/near the ecliptic plane. A range of 2.5% to 12.7% was found by Smith (1973a), Neugebauer et al. (1984) and Lepping and Behannon (1986) for in-ecliptic data analyses. Thus the TD occurrence rate at high heliographic latitudes is surprisingly large, percentage wise.

Nature of Tangential Discontinuities

TDs have been detected at the edges in dips in the magnetic field magnitude. These dips have previously been named magnetic holes by (Turner et al., 1977) and have been recently related to mirror mode structures (Tsurutani et al., 1982) by Winterhalter et al. (1994) and Ho et al. (1995). Typically there is pressure balance across the holes. It is generally found that the plasma in adjacent regions to the holes were stable against the mirror instability and unstable within the hole. The instability criterion is:

$$R=(\beta_\perp/\beta_\parallel)/(1+1/\beta_\perp)$$

where the plasma "beta" $\beta=8\pi\Sigma_i N_i kT_i/|B|^2$ and the "Σ_i" in the plasma pressure is over all ion species and electrons. "$\perp$" and "$\parallel$" indicate components perpendicular and parallel to the ambient magnetic field direction.

An example of a hole is shown in Figure 16, taken from Winterhalter et al. (1994) and the tangential discontinuity at the edge of a hole with the instability criteria plotted simultaneously (from Ho et al., 1995), Figure 17. Note that the mirror instability is satisfied within the hole, but not outside it.

In the Turner et al. (1997) work, their holes were isolated structures. However one often finds more complex structures like that shown in Figure 17. When the field decrease structures are complex, there are typically only discontinuities at the two edges of the major structure. There are generally few TDs with these complex holes.

It is believed that because of the plasma is stable to the mirror mode in the region adjacent to the holes, the instability may have occurred closer to the sun and these structures are simply plasma "fossils" that are being convected outward into the distant heliosphere. However, it should be noted that within a hole, where $\beta >> 1$, the instability criteria becomes $\cong \beta_{\perp} / \beta_{\parallel} > 1$, which is relatively easy to satisfy. Here the fact that mirror instability is met within holes may be fortuitous. These structures could be a result of other plasma processes as well.

Ho et al. (1995) detected current sheet-related TDs. This is shown in Figure 18. In this event the current sheet was located on the gradient of a microstream. However, not all current-sheet related TDs were found to be so related.

The multilayer structure of TD has been reproduced by a kinetic model (DeKeyser et al., 1996a). A generalized Vlasov model is used. A best choice is selected for the velocity distribution function and therefore "predicts" the plasma parameters in the absence of high-time resolution plasma measurements.

Figure 19 shows one simulation of a TD. There are several current layers with current density of the order of 3×10^{-11} A m^{-2}. There is an electrostatic potential of less than 50 mV, indicating an extremely weak field along its normal. DeKeyser et al. comment that such models do not address issues of particle accessibility and also mention that the current layers with large shears and/or gradients may be unstable to the growth of electromagnetic plasma waves and may be in a state of turbulence rather than equilibrium.

Another work by DeKeyser et al. (1996b) has implied non-Maxwellian electron and ion velocity distribution functions within the transition layer. The nonconstant solar wind bulk velocity is a major reason why the plasma develops current carrying boundary layers.

Slow Shocks

One of the rarest of discontinuities in interplanetary are shocks. Of the various types of shocks (fast, intermediate and slow), slow mode shocks are the rarest. Over the last few decades of interplanetary space missions, only a few have been reported in the literature (Chao and Olbert, 1970; Richter, 1991). The reason for the rarity is most probably that slow-mode shocks develop in regions where collisionless damping of slow mode waves is small and the damping time exceeds the wave steepening time. This requires that plasma $\beta < 1$ and $T_p/T_e < 1$, conditions not typically found interplanetary space.

However in the Ulysses data, some slow shocks have been detected, and in fact, a slow shock pair (forward and reverse) has been found for the first time! This pair of slow-mode shocks is located embedded within a CIR where the above plasma conditions were met (at 5.3 AU and 9° S heliolatitude). It is possible that at even larger radial distances slow mode shocks may be even more common.

Figure 20 shows the plasma and field data for the shock pair (from Ho et al., 1998). The two shock discontinuities are denoted by the vertical lines. The forward slow shock occurs at 0710 UT and the reverse slow shock at 1105 UT. At the first event, V_{SW} increases from 425 to 463 km s^{-1}, N_p from 0.6 to 1.2 cm^{-3}, and T_p from 0.4 to 0.5 x 10^5 K. |B| decrease from 1.4 to 1.1 nT. At the second discontinuity, V_{SW} increase from 447 to 500 km s^{-1}, N_p decreases from 0.2 to 0.07 cm^{-3}, and T_p decrease from 1.5 to 0.6 x 10^5 K. |B| increases from 1.2 to 1.7 nT. The shock speeds have been calculated to be 60 km s^{-1} and 115 km s^{-1}, respectively. These speeds are not unlike those of Ulysses fast-mode shocks at these distances.

These slow mode shocks may be associated with magnetic field reconnection. Energetic 30-90 keV electron and ion acoustic-like plasma waves were associated with this event. This may be one form of magnetic energy dissipation.

Alfvén Waves and Geomagnetic Activity at the Earth

In the ecliptic plane, fast corotating solar wind streams (~750-800 km s^{-1}) emanating from coronal holes will overtake the slower streams (~350-400 km s^{-1}). The "collision" between the

streams will lead to a region of compressed magnetic fields and plasma. This compressed region of fields are called "corotating interaction regions" or CIRs (Smith and Wolf, 1976). When CIRs are detected far from the Sun, they are bounded by fast forward (FS) and fast reverse (RS) shocks, and the fast and slow stream material are separated by an interface surface (IF) generally believed to be a TD. However closer to the sun, near the Earth at 1 AU, CIRs typically do not have either forward or reverse shocks (Tsurutani et al. 1995a). The Alfvén waves in the high-speed streams appear to be compressed as they cross the reverse shock, i.e., their amplitudes are magnified. A schematic for the above discussion is shown in Figure 21.

Interplanetary Alfvénic (transverse) fluctuations appear to be more or less random in direction. However, when the fluctuations happen to be in the north-south direction, they can have very important geophysical consequences. Southward directed IMFs will allow connection between the interplanetary magnetic fields and the Earth's magnetopause (northward directed) magnetic fields (Dungey, 1961). Connection allows an input of solar wind energy into the magnetosphere/magnetotail system and results in energy injection into the nightside magnetosphere and ionosphere in the form of substorms. The relationship between these southward components and a nightside auroral electrojet (AE) index is shown in Figure 22. For each southward turning, the AE index increases, indicating substorm activity and auroral particle precipitation.

During the declining phase of the solar cycle, polar coronal holes become large and migrate down to equatorial latitudes. When coronal holes from both poles are present at the equator (such as during 1973-1975), two high-speed streams impact the Earth's magnetosphere each 27-day solar rotation. Under these conditions, the input of solar wind energy into the magnetosphere is exceptionally high, higher than during solar maximum. In 1974, the average AE was 283 nT compared to only 221 nT in 1979 (solar maximum). Although there were many more intense ($D_{ST} < -100$ nT) magnetic storms during 1979 than during 1974, these are episodic events and only contribute a small amount of energy in comparison to the almost continuous energy injection due to the Alfvén waves and resultant High Intensity, Long-Duration Continuous Auroral Activity (HILDCAAs) events.

SUMMARY/FOREFRONTS

Many new discoveries concerning interplanetary discontinuities were made by the Ulysses mission. The discovery that the RDs were the phase steepened edges of nonlinear Alfvén waves was one of the major finds of the Mission. The consequences of such features in the

interplanetary medium is currently being explored. In fact, nonlinear waves and wave phase steepening are part of a new emerging field in plasma physics. A merger of space plasma, fusion plasma and mathematicians are hard at work grappling with both theory and observations to try to understand these features (Hada and Matsumoto, 1996).

Besides the problems listed above, there is still much more to do and learn. It is not understood why perfect, ideal RDs ($\Delta|B|/B_L = 0$ and $B_n/B_L = 1$) and perfect TDs ($\Delta|B|/B_L$ and $B_n/B_L = 0$) exist only rarely in nature. Such pure TDs and RDs are generally not found in interplanetary space. The reason for this is not known.

So far only two regions of discontinuity phase space have been dealt with. In Figure 15, the region $\Delta|B|/B_L > 0.2$ and $B_N/B_L > 0.2$ has not been studied. This region of phase space is ordinarily thought to be the region where interplanetary shocks are found. However, clearly fast forward shocks are not present at these high latitudes. These discontinuities must be due to some other phenomenon. This needs to be investigated further.

The region of $\Delta|B|/B_L < 0.2$ and $B_N/B_L < 0.4$ also needs to be studied. Neugebauer et al. (1984) using field and plasma data, found that many of the discontinuities with "properties of both TDs and RDs" were in actuality mainly RDs.

One clear outstanding problem is the determination of the direction of propagation of RDs. Figure 23 shows the minimum variance direction of the discontinuities from days 154-155, 1995 in the RTN coordinate system. This pattern looks quite isotropic, a somewhat surprising outcome. However, it should be noted that for arc-polarized structures, almost all of the variance will be in the B_1 direction with very little in B_2. Thus the ratio of λ_2/λ_3 will be generally close to 1.0, making the uncertainty in determination quite large. There is also a physical problem with this issue as well. If, as everyone has agreed, the Alfvén waves are propagating radially outward, then the leading or trailing edges should be directed in the antisunward or sunward directions, respectively. The minimum variance direction is more or less isotropic as has been noted and individual examples have indicated directions orthogonal to the radial.

Tsurutani (1997) in examining this issue, believe that for spherical waves, the minimum variance direction may not be the direction of propagation, but the intermediate variance direction instead. Arguments have been made why an orthogonal directionality would imply a left-hand and a right-hand wave coupling, which would soon dispersively separate. Thus the RDs would soon pull away from the slowly rotating part of the Alfvén wave. Currently mutlispacecraft studies

are focusing on this topic. The ultimate answer might come when the Cluster mission finally gets launched.

Acknowledgments. Portions of this work were performed at the Jet Propulsion Laboratory, California Institute of Technology, Pasadena, under contract with the National Aeronautics and Space Administration.

References

Balogh, A., E.J. Smith, B.T. Tsurutani, D.J. Southwood, R.J. Forsyth and T.S. Horbury, The heliospheric magnetic field over the south polar region of the sun, *Science, 268*, 945, 1995.

Behannon, K.W., Heliocentric distance dependence of the interplanetary magnetic field, *Rev. Geophys., 16*, 125, 1978.

Belcher, J.W. and L. Davis, Jr., Large amplitude Alfvén waves in the interplanetary medium, 2, *J. Geophys. Res., 76*, 3534, 1971.

Burlaga, L.F., Nature and origin of directional discontinuities in the solar wind, *J. Geophys. Res., 76*, 4360, 1971.

Buti, B., V.L. Galinski, V.I. Shevchenko, G.S. Lakhina, B.T. Tsurutani, P. Diamond and M.V. Medvedev, Evolution of nonlinear Alfvén waves in streaming inhomogeneous plasmas, *Astrophys. J.*, 1998.

Buti, B., V. Jayanti, A.F. Vinas, G.S. Ghosh, M.L. Goldstein, D.A. Roberts, G.S. Lakhina and B.T. Tsurutani, Nonlinear evolution of Alfvén wave packets, submitted to *Geophys. Res. Lett.*, 1998.

Chao, J.K. and S. Olbert, Observation of slow shocks in interplanetary space, *J. Geophys. Res., 75*, 6394, 1970.

DeKeyser, J., M. Roth, J. Lemaire, B.T. Tsurutani, C.M. Ho and C.M. Hammond, Theoretical plasma distributions consistent with Ulysses magnetic field observations in a solar wind tangential discontinuity, *Solar Phys, 166*, 415, 1996.

DeKeyser, J., M. Roth, B.T. Tsurutani, C.M. Ho and J.L. Phillips, Solar wind velocity jumps across tangential discontinuities: Ulysses observations and kinetic interpretation, *Astron. Astrophys. 166*, 415, 1996.

Dungey, J.W., Interplanetary magnetic field and the auroral zones, *Phys. Res. Lett., 6*, 47, 1961.

Hada, T. and H. Matsumoto, *Nonlinear Waves and Chaos in Space Plasmas*, Terra Scientific, Tokyo, 1997.

Ho, C.M., B. T. Tsurutani, B.E. Goldstein, J.L. Phillips and A. Balogh, Tangential discontinuities at high heliographic latitudes (~ −80°), *Geophys. Res. Lett., 22*, 3409, 1995.

Ho, C.M., B.T. Tsurutani, N. Lin, L.J. Lanzerotti, E.J. Smith, B.E. Goldstein, B. Buti, G. S. Lakhina and X.Y. Zhou, A pair of forward and reverse slow-mode shocks detected by Ulysses at ~5 AU, *Geophys, Res. Lett.*, 1998.

Kennel, C.F. and H.E. Petschek, Limit on stably trapped particle fluxes, J. *Geophys. Res., 71*, 1, 1996.

Lepping, R.P. and K.W. Behannon, Magnetic field directional discontinuities: Characteristics between 0.46 and 1.0 AU, *J. Geophys. Res., 91*, 8725, 1986.

Mariani, F., B. Bavassano, U. Villante and N.F. Ness, Variation of the occurrence rates of discontinuities in the interplanetary magnetic field, *J. Geophys. Res., 78*, 8011, 1973.

Medvedev, M.V., P.H. Diamond, V.I. Shevchenko, and V.L. Galinsky, Dissipative dynamics of collisionless nonlinear Alfvén wave trains, *Phys. Rev. Lett.*, 1998.

Neugebauer, M., B.E. Goldstein, D.J. McComas, S.T. Suess, and A. Balogh, Ulysses observations of microstreams in the solar wind from coronal holes, *J. Geophys. Res., 100*, 23389, 1995.

Neugebauer, M., D.R. Clay, B.E. Goldstein, B.T. Tsurutani and R.D. Zwickl, A re-examination of rotational and tangential discontinuities in the solar wind, *J. Geophys. Res., 89*, 5395, 1984.

Phillips, J.L., A. Balogh, S.J. Bame, B.E. Goldstein, J.T. Gosling, J.T. Hoeksema, D.J. McComas, M. Neugebauer, N.R. Sheeley, Jr. and Y. M. Wang, Ulysses at 50° south: Constant immersion in the high speed solar wind, *Geophys. Res. Lett., 21*, 1105, 1994.

Richter, A.K., Interplanetary slow shocks, Space and Solar Physics, *21*, 23, *Physics of the Inner Heliosphere II*, R. Schwenn and E. Marsch, editors, Springer-Verlag, Heidelberg, 1991.

Riley, P., C.P. Sonett, B. T. Tsurutani A. Balogh, R.J. Forsyth and G.W. Hoogeveen, Properties of arc-polarized Alfvén waves in the ecliptic plane: Ulysses observations, *J. Geophys. Res., 101*, 19987, 1996.

Smith, E.J., Identification of interplanetary tangential and rotational discontinuities, *J. Geophys. Res., 78*, 2054, 1973a.

Smith, E.J., Observed properties of interplanetary rotational discontinuities, *J. Geophys. Res., 78*, 2088, 1973b.

Smith, E.J. and J.H. Wolf, Observations of interaction regions and corotating shocks between one and five AU: Pioneers 10 and 11, *Geophys. Res. Lett., 3*, 137, 1976.

Smith, E.J., M. Neugebauer, A. Balogh, S.J. Bame, G. Erdos, R.J. Forsyth, B. E. Goldstein, J.L. Phillips, and B.T. Tsurutani, Disappearance of the heliospheric sector structure at Ulysses, *Geophys. Res. Lett., 20*, 2327, 1993.

Smith, E.J., A. Balogh, M. Neugebauer, and D. McComas, Ulysses observations of Alfvén waves in the southern and northern hemispheres, *Geophys. Res. Lett., 22*, 3381, 1995.

Tsurutani, B.T. and E.J. Smith, Interplanetary discontinuities: Temporal variations and the radial gradient from 1 to 8.5 AU, *J. Geophys. Res., 84*, 2773, 1979.

Tsurutani, B.T., E.J. Smith, R.R. Anderson, K.W. Ogilvie, J.D. Scudder, D.N. Baker, and S.J. Bame, Lion roars and nonoscillatory drift mirror waves in the magnetosheath, *J. Geophys. Res., 87*, 6060, 1982.

Tsurutani, B.T., C.M. Ho, E.J. Smith, M. Neugebauer, B.E. Goldstein, J.S. Mok, J.K. Arballo, A. Balogh, D.J. Southwood and W. C. Feldman, The relationship between interplanetary discontinuities and Alfvén waves: Ulysses observations, *Geophys. Res. Lett., 21*, 2267, 1994.

Tsurutani, B.T., C.M. Ho, J.K. Arballo, B.E. Goldstein, Large amplitude IMF fluctuations in corotating interaction regions: Ulysses at midlatitudes *Geophys. Res. Lett., 22*, 3397, 1995a.

Tsurutani, B.T., W. D. Gonzalez, A.L.C. Gonzalez, F. Tang, J.K. Arballo and M. Okada, Interplanetary origin of geomagnetic activity in the declining phase of the solar cycle, *J. Geophys. Res., 100*, 21717, 1995b.

Tsurutani, B.T., C.M. Ho, J.K. Arballo, E.J. Smith, B.E. Goldstein, M. Neugebauer, A. Balogh, and W.C. Feldman, Interplanetary discontinuities and Alfvén waves at high heliographic latitudes: Ulysses, *J. Geophys. Res., 101*, 11027, 1996.

Tsurutani, B.T., C.M. Ho, R. Sakurai, B.E. Goldstein, A. Balogh and J.L. Phillips, Symmetry in discontinuity properties at the north and south heliospheric poles: Ulysses, *Astron.* and *Astrophys. 316*, 342, 1996.

Tsurutani, B.T., K.-H. Glassmeier and F.M. Neubauer, A review of nonlinear low frequency (LF) wave observations in space plasmas: On the development of plasma turbulence, *in Nonlinear Waves and Chaos in Space Plasmas*, edited by T. Hada and H. Matsumoto, Terra Scientific, Tokyo, 1, 1997a.

Tsurutani, B.T., C.M. Ho, J.K. Arballo, G.S. Lakhina, K.-H. Glassmeier and F.M. Neubauer, Nonlinear electromagnetic waves and spherical arc-polarized waves in space plasmas, *Plasma Phys. Controlled Fusion, 39*, A237, 1997b.

Tsurutani, B.T. and G.S. Lakhina, Some basic concepts of wave-particle interactions in collisionless plasmas, *Rev. Geophysics, 35*, 491, 1997.

Turner, J.M., L.F. Burlaga, N.F. Ness and J.F. Lemaire, Magnetic holes in the solar wind, *J. Geophys. Res., 82*, 1921, 1997.

Vasquez, B.J. and J.V. Hollweg, Formation of spherically polarized Alfvén waves and embedded rotational discontinuities from a small number of entirely oblique waves, *J. Geophys. Res. 103*, 335, 1998a.

Vasquez, B.J. and J.V. Hollweg, Formation of embedded rotational discontinuities with nearly field-aligned normals, *J. Geophys. Res., 103*, 349, 1998b.

Winterhalter, D., M. Neugebauer, B.E. Goldstein, E.J. Smith, B.T. Tsurutani, S.J. Bame and A. Balogh, Magnetic holes in the solar wind and their relation to mirror-mode structures, *Space Sci. Rev.*, Kluwer, Netherlands, 72, 201, 1995.

Figure Captions

Figure 1. Mass flux and magnetic field change across idealized discontinuities.

Figure 2. Schematics of idealized rotational and tangential discontinuities. From Tsurutani et al. (1997a).

Figure 3. The in-ecliptic rate of occurrences of interplanetary discontinuities (ROID) values from 1 to 5 AU. The solid curve is the results of the TS criteria and the dashed curve that of the LB criteria.

Figure 4. The solar wind plasma and magnetic field and rate of interplanetary discontinuity (ROID) values for the TS and LB criteria, from Tsurutani et al. (1996a).

Figure 5. Nonlinear $(\Delta\vec{B}/|B|\sim 1-2)$ Alfvénic fluctuations for July 1994. These fluctuations are characteristic of high-speed streams emanating from polar coronal holes. From Tsurutani et al. (1996a).

Figure 6. The $B_R - V_R, B_T - V_T, B_N - V_N$ cross-correlation coefficients for the interval in Figure 5.

Figure 7. Comparison of normalized magnetic field power spectra over the solar pole (−79° latitude) in a high-speed stream in the ecliptic (−1.9°) latitude)plane.

Figure 8. The temporal (top panel) and spatial (bottom panel) "thicknesses" of interplanetary discontinuities at −67° latitude and 3.0 AU. The spatial thickness for each individual discontinuity determined by dividing the temporal "thickness" by the solar wind velocity. The discontinuity normal direction was also taken into account. From Tsurutani et al. (1996a).

Figure 9. The magnetic field at 5.2 AU at −6.0° latitude. Many of the TS selected discontinuities (vertical lines) occur at the edges of the more slowly rotating Alfvén waves. From Tsurutani et al. (1997a).

Figure 10. The relationship between a rotational discontinuity (between points 2 and 3) and a slowly rotating Alfvén waves (between points 1 and 2). The rotational discontinuity is the phase-steepened edge of the Alfvén wave. The wave is arc-polarized and to first order, noncompressive.

Figure 11. In panel a), B_{int} is plotted against B_{max} for a 2 hour, 40 minute interval of day 250, 1991. Panel b), a 3-d display of the same data in panel a). Panel c), B_{nin} and |B|. From Riley et al (1996).

Figure 12. The different possible polarizations for plane waves (left-hand panel) and spherical waves (right-hand panel).

Figure 13. The normalized jumps in field magnitude, density and temperature across rotational discontinuities. In each case, the difference value is normalized by dividing by the sunward "downstream" value.

Figure 14. A comparison of discontinuity occurrence rates over the north pole and over the south pole. From top to bottom are the average solar wind densities, temperatures, velocities, magnetic field magnitudes, TS ROID values, and Ulysses heliocentric radial distances and latitudes. All ROID values are relatively constant. If the different radial distances of the two Ulysses passes are taken into account, there is no obvious asymmetry present. From Tsurutani et al. (1996b).

Figure 15. Discontinuity phase spaces (B_3/B_L, $\Delta|B|/B_L$) distributions for days 218-221, 1993 at the north heliographic pole.

Figure 16. Examples of "magnetic holes". $B_{min}/B_0 < 0.5$ and $\delta\theta < 5°$ (linear holes) for both cases.

Figure 17. An example of a TD at the edge of mirror mode related field decreases. Note that the field decreases are complex and not as nicely ordered as for mirror mode structures detected in planetary magnetosheaths. Taken from Ho et al. (1995).

Figure 18. A current-sheet related TD on day 239, 1994. Ulysses was at −79.3° heliographic latitude. This event occurred at the gradient of a microstream. Taken from Ho et al. (1995).

Figure 19. Observed (dashed lines) and simulated (solid lines) of two components of the field in minimum variance coordinates (rotated for convenience by −15°along the X-axis). The normal field (B_X) is less than 15% of B magnitude. two dashed vertical lines delimit the TD crossing centered at 0529 UT July 3, 1993. In the RTN coordinate system, the normal is 0.96, −0.05, −0.30, indicating that the TD was essentially orthogonal to the solar wind velocity vector. Taken from DeKeyser et al. (1996).

Figure 20. From top to bottom are: the solar wind speed, proton density, proton temperature, magnetic field components in solar-heliospheric coordinates, field magnitude, plasma beta and proton to electron temperature ratios.

Figure 21. The discontinuity normals for days 154-155, 1994. The normals are displayed in the RTN coordinate system. Taken from Tsurutani et al. (1996a).

Figure 22. The interaction of a high-speed stream (B) with a slow-speed stream (A) and the corotating interaction region (CIR) formed (shaded). The Alfvén waves present in the high-speed stream proper (B) will be compressed as they are swept up by the expanding reverse shock.

Figure 23. The IMF B magnitude, B_Z, AE and D_{ST} for day 136, 1974. Increases in B_S and AE and slightly delayed decreases in D_{ST} are illustrated.

Tables

Table 1. Seven two-day intervals at a variety of heliocentric latitude used to intercompare interplanetary "Alfvénicity". The average field magnitude, solar wind velocity, proton density and proton temperature are given.

Type of Discontinuity	Mass Flux ρv_n	Change in Magnetic Field $[\vec{H}]$	
Contact Discontinuity	0	$[\vec{H}_T] = 0$	$H_n \neq 0$
Tangential Discontinuity	0	$[\vec{H}_T] \neq 0$	$H_n = 0$
Rotational Discontinuity	$\neq 0$	$[H_T] = 0$	$H_n \neq 0$
Shock	$\neq 0$	$[\vec{H}_T] \neq 0$ $[H_T] \neq 0$	$H_n \neq 0$

Fig 1

TANGENTIAL DISCONTINUITY

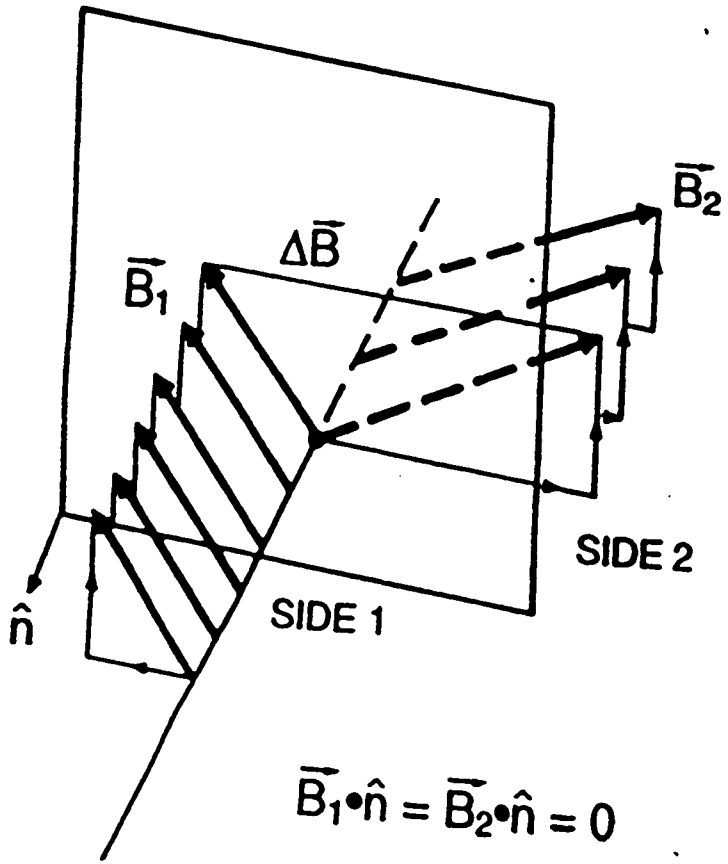

$$\vec{B}_1 \cdot \hat{n} = \vec{B}_2 \cdot \hat{n} = 0$$

ROTATIONAL DISCONTINUITY

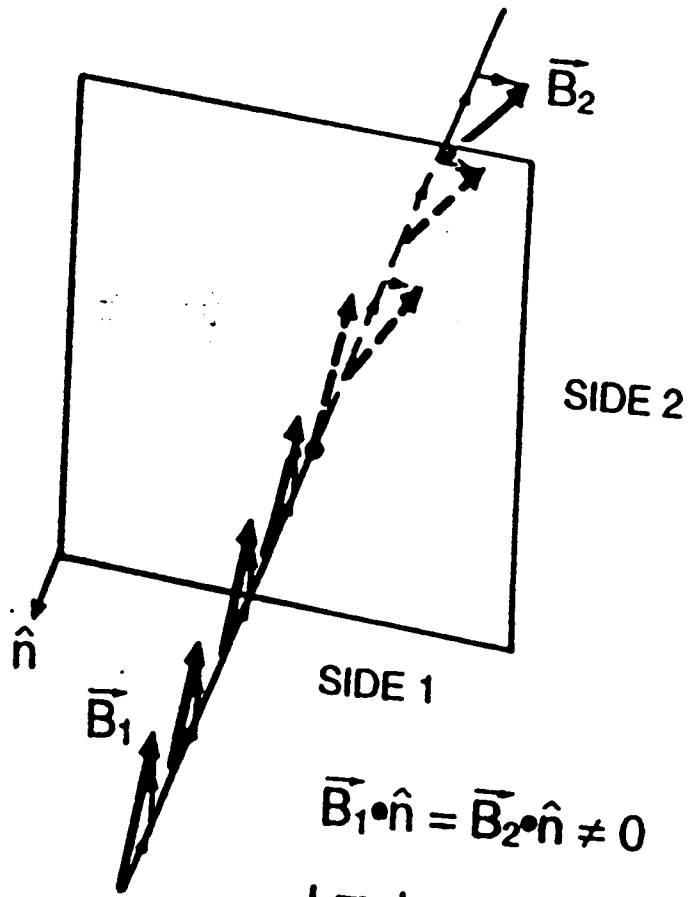

$$\vec{B}_1 \cdot \hat{n} = \vec{B}_2 \cdot \hat{n} \neq 0$$

$$|\vec{B}_1| = |\vec{B}_2|$$

Fig 2

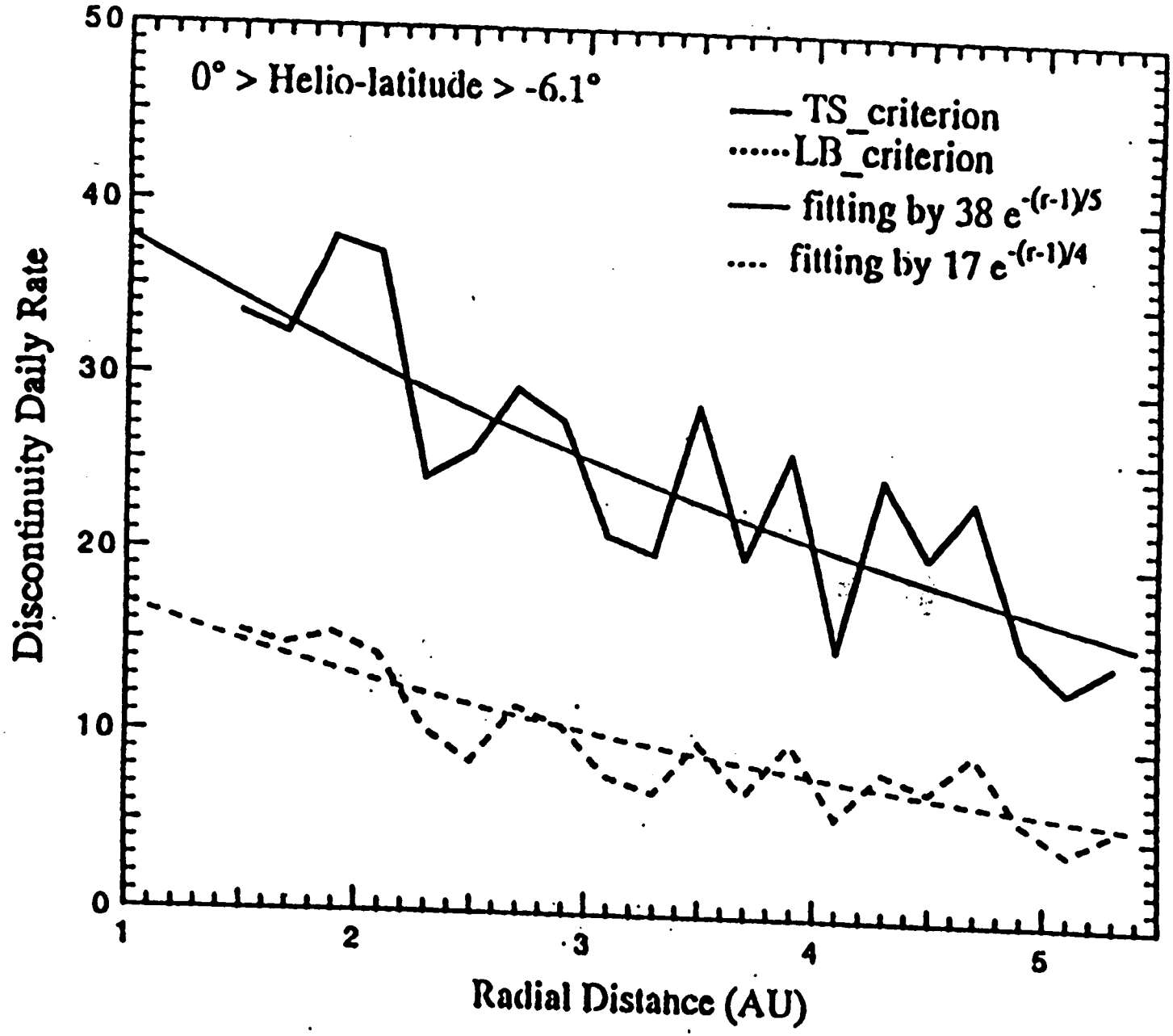
0° > Helio-latitude > -6.1°
TS_criterion
LB_criterion
fitting by 38 e^-(r-1)/5
fitting by 17 e^-(r-1)/4
Discontinuity Daily Rate
Radial Distance (AU)
0
10
20
30
40
50
1
2
3
4
5

Fig 3

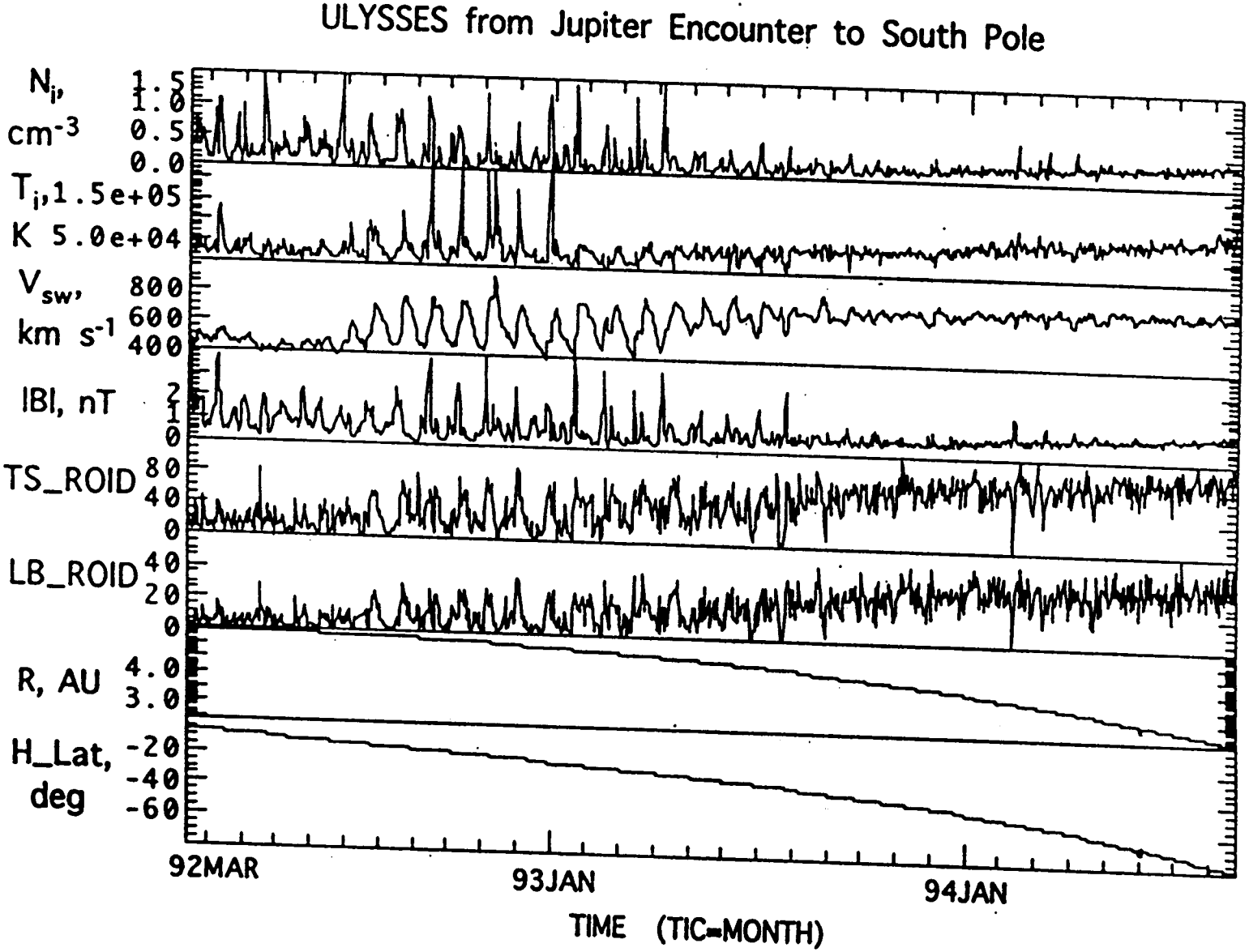
ULYSSES from Jupiter Encounter to South Pole
N_i, cm^{-3}
1.5
1.0
0.5
0.0
T_i, K
1.5e+05
5.0e+04
V_{sw}, km s^{-1}
800
600
400
IBI, nT
2
1
0
TS_ROID
80
40
0
LB_ROID
40
20
0
R, AU
4.0
3.0
H_Lat, deg
-20
-40
-60
92MAR
93JAN
94JAN
TIME (TIC=MONTH)

Fig 4

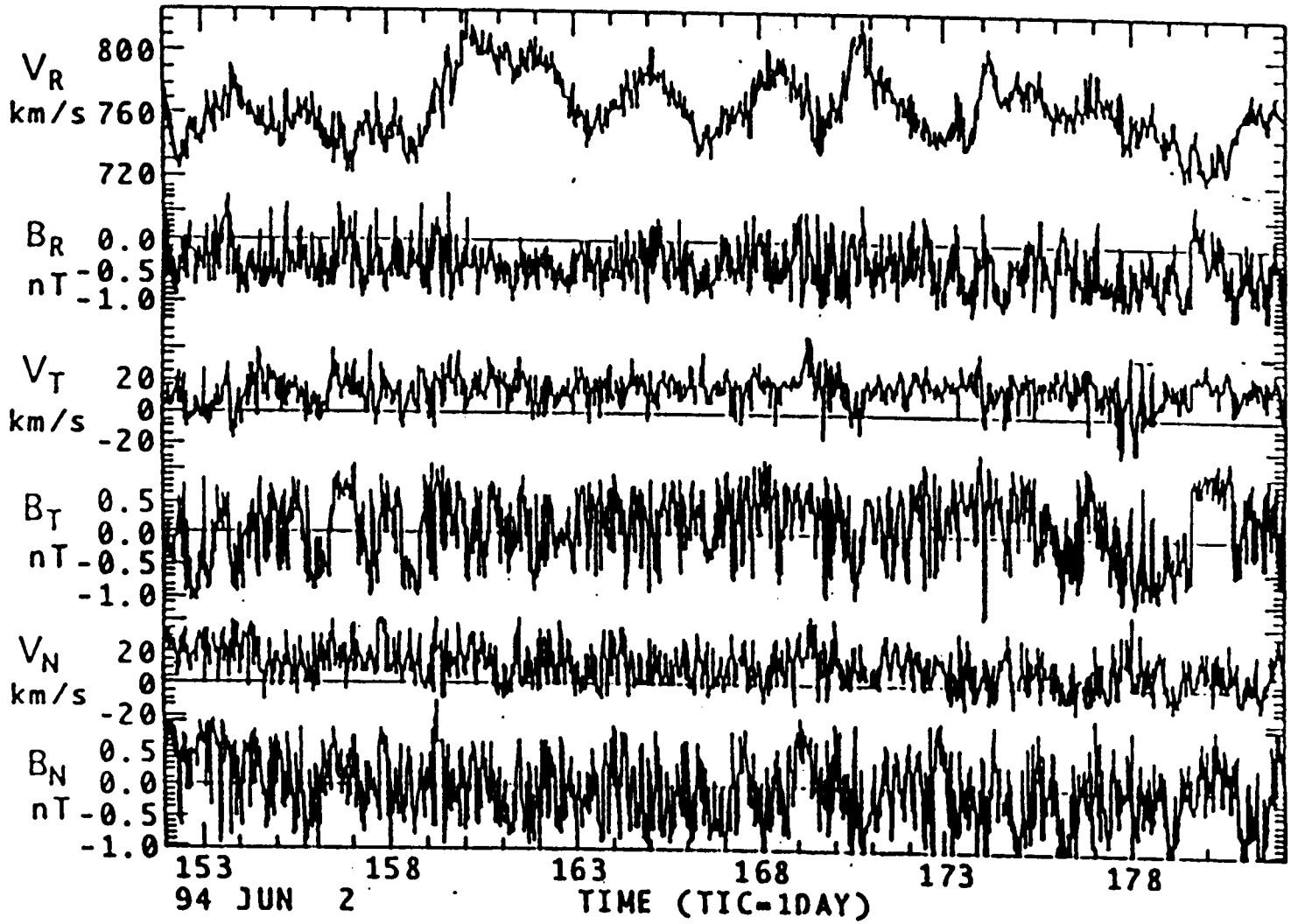
V_R
km/s
800
760
720
B_R
nT
0.0
-0.5
-1.0
V_T
km/s
20
0
-20
B_T
nT
0.5
0.0
-0.5
-1.0
V_N
km/s
20
0
-20
B_N
nT
0.5
0.0
-0.5
-1.0
153
158
163
168
173
178
94 JUN 2
TIME (TIC-1DAY)

Fig 5

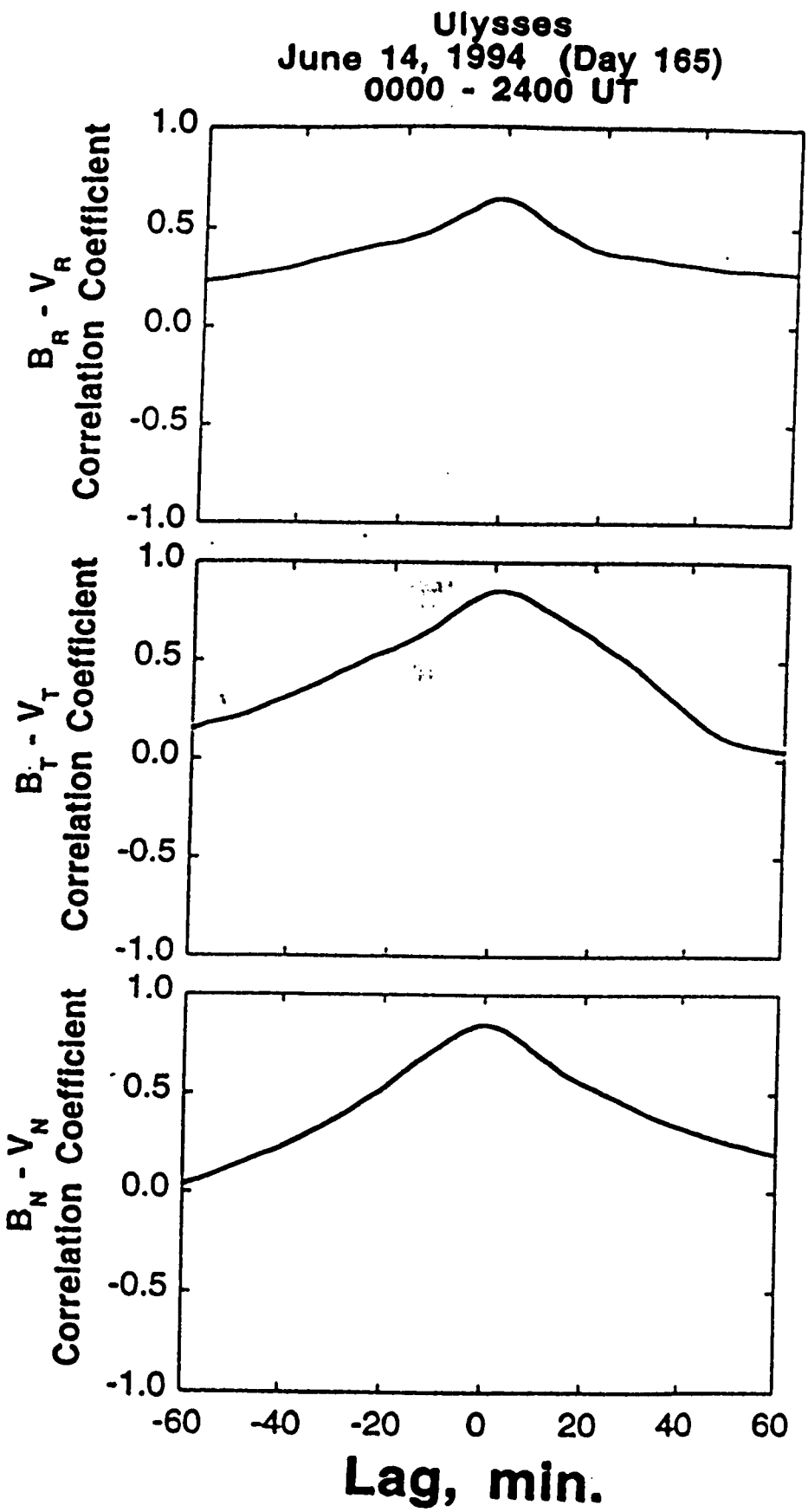
Ulysses
June 14, 1994 (Day 165)
0000 - 2400 UT
B_R - V_R Correlation Coefficient
B_T - V_T Correlation Coefficient
B_N - V_N Correlation Coefficient
1.0
0.5
0.0
-0.5
-1.0
-60
-40
-20
0
20
40
60
Lag, min.

Fig 6

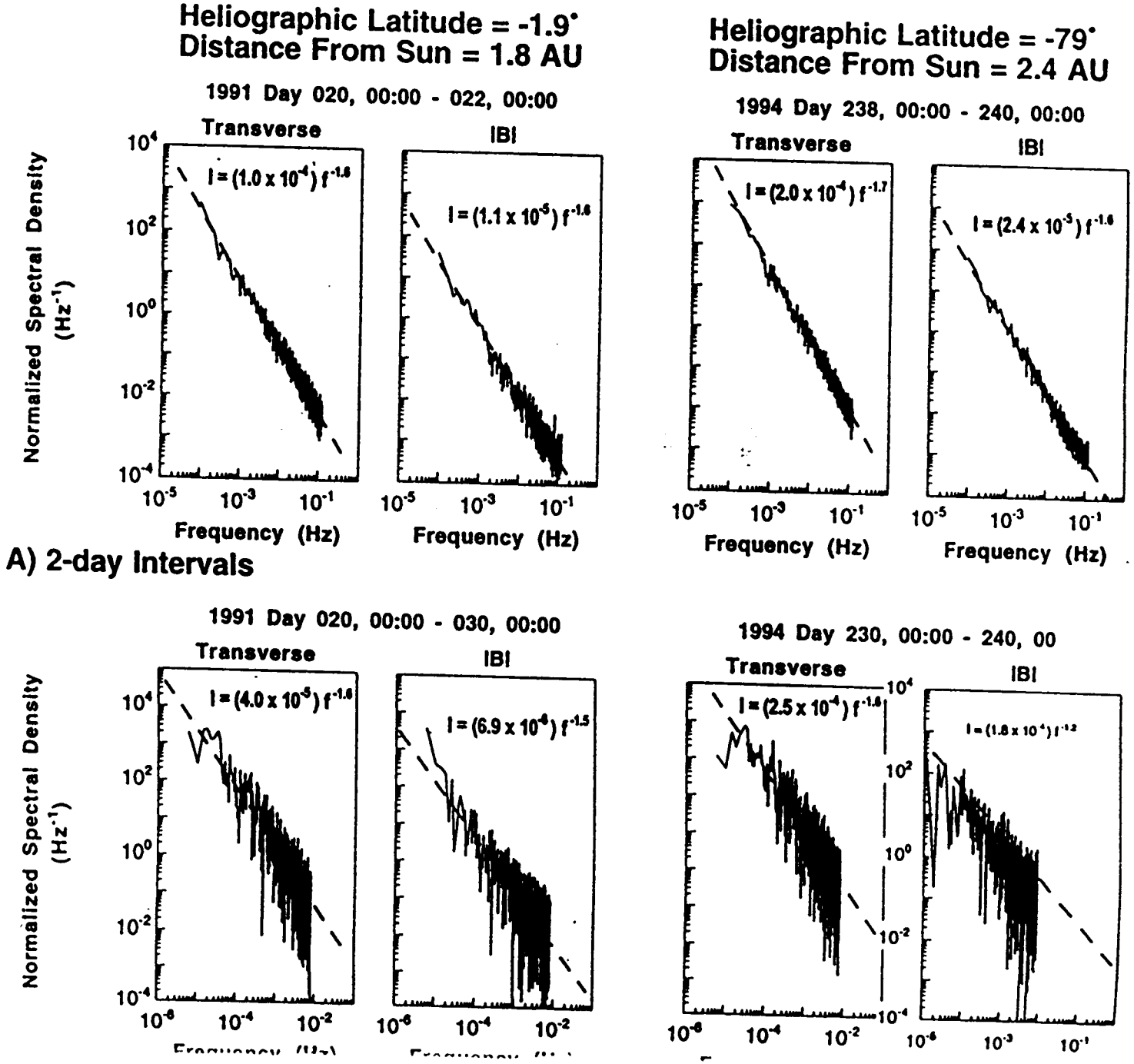
Heliographic Latitude = -1.9°
Distance From Sun = 1.8 AU
1991 Day 020, 00:00 - 022, 00:00
Transverse
IBI
I = (1.0 x 10⁻⁴) f⁻¹·⁶
I = (1.1 x 10⁻⁵) f⁻¹·⁶
Normalized Spectral Density (Hz⁻¹)
Frequency (Hz)
Heliographic Latitude = -79°
Distance From Sun = 2.4 AU
1994 Day 238, 00:00 - 240, 00:00
I = (2.0 x 10⁻⁴) f⁻¹·⁷
I = (2.4 x 10⁻⁵) f⁻¹·⁶
A) 2-day Intervals
1991 Day 020, 00:00 - 030, 00:00
I = (4.0 x 10⁻⁵) f⁻¹·⁶
I = (6.9 x 10⁻⁶) f⁻¹·⁵
1994 Day 230, 00:00 - 240, 00
I = (2.5 x 10⁻⁴) f⁻¹·⁶

Fig 7

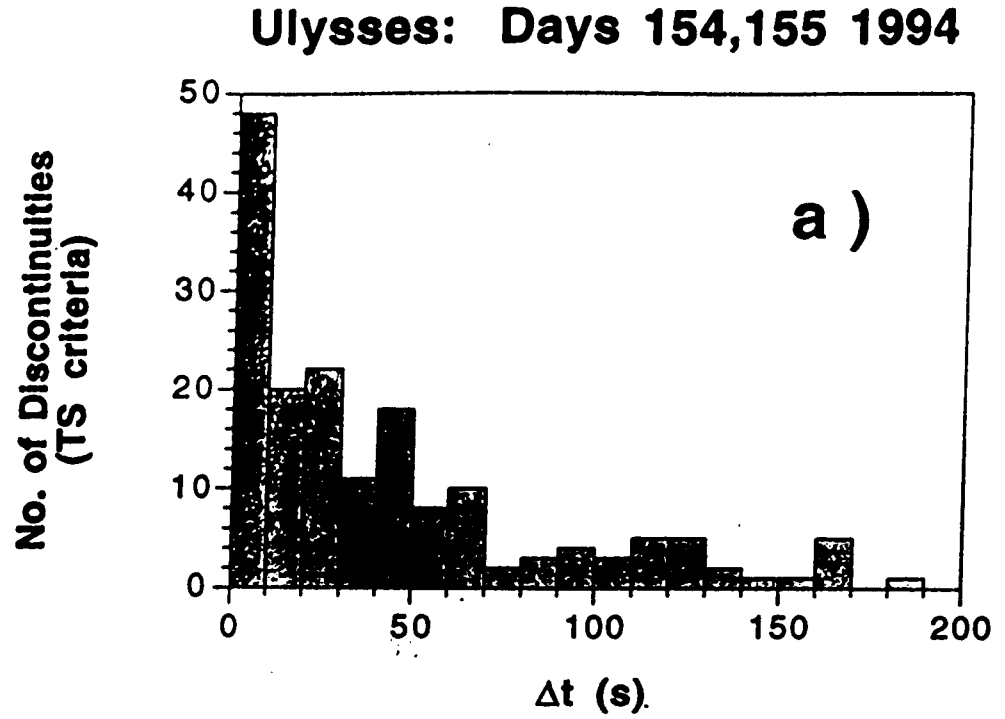
Ulysses: Days 154,155 1994
No. of Discontinuities (TS criteria)
a)
0
10
20
30
40
50
0
50
100
150
200
Δt (s)

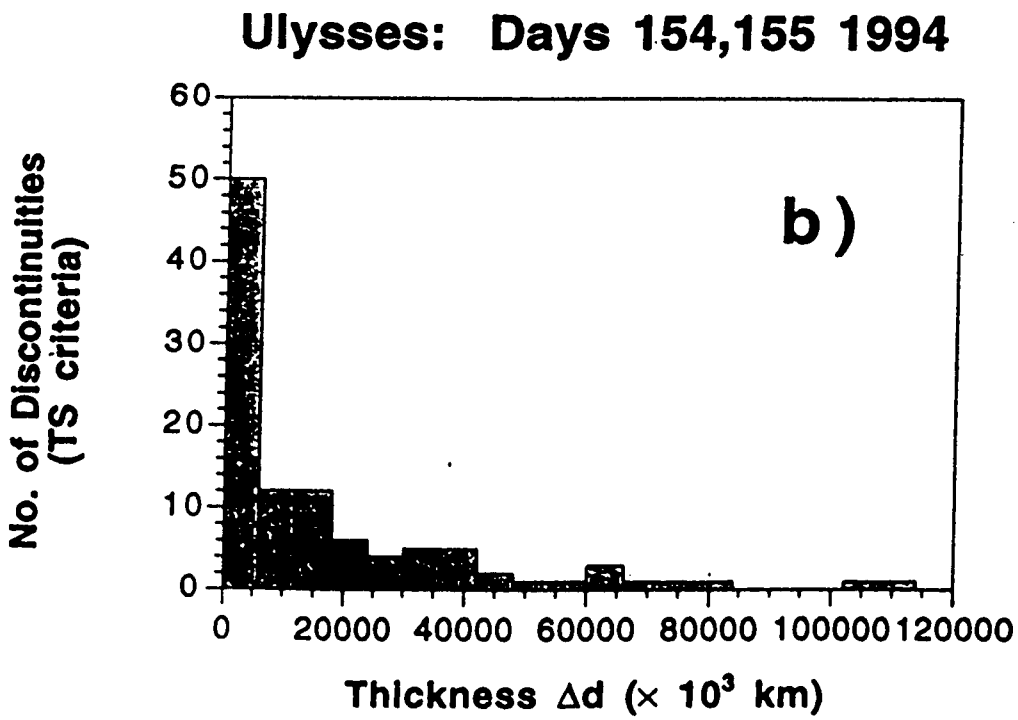
Ulysses: Days 154,155 1994
No. of Discontinuities (TS criteria)
b)
0
10
20
30
40
50
60
0
20000
40000
60000
80000
100000
120000
Thickness Δd (× 10³ km)

Fig 8

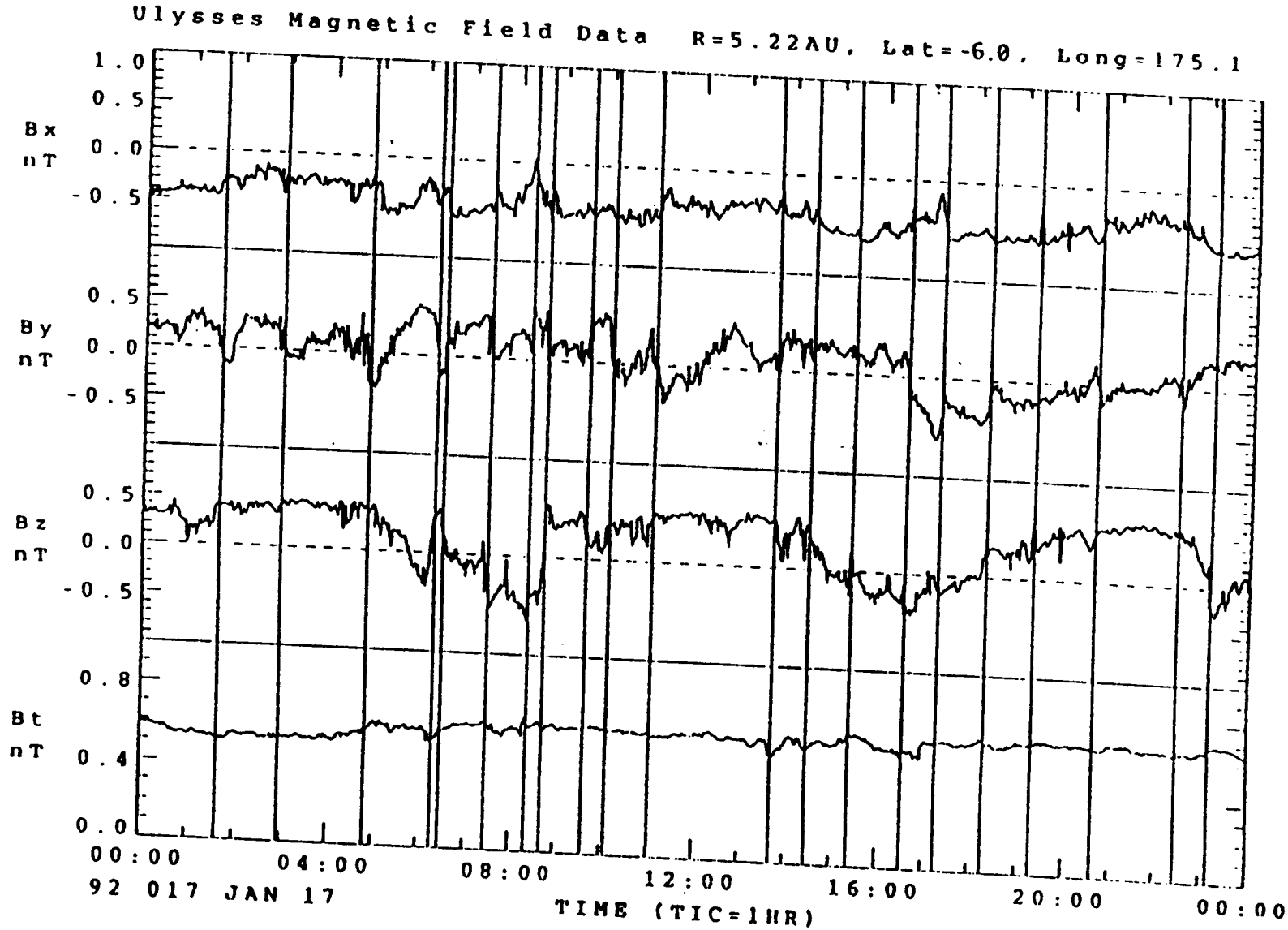
Ulysses Magnetic Field Data R=5.22AU, Lat=-6.0, Long=175.1
Bx nT
1.0
0.5
0.0
-0.5
By nT
0.5
0.0
-0.5
Bz nT
0.5
0.0
-0.5
Bt nT
0.8
0.4
0.0
00:00
04:00
08:00
12:00
16:00
20:00
00:00
92 017 JAN 17
TIME (TIC=1HR)

Fig 9

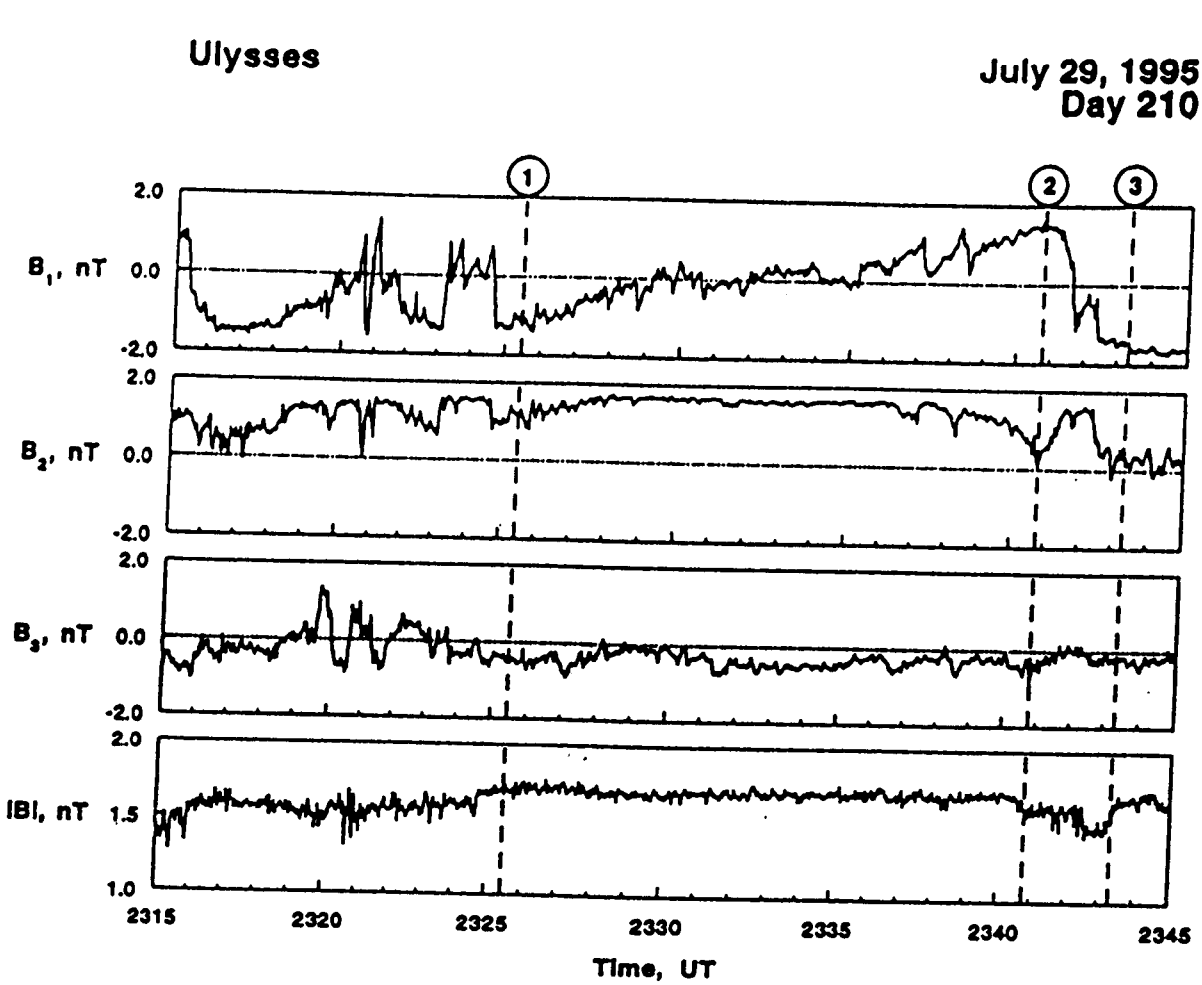
Ulysses
July 29, 1995
Day 210
1
2
3
2.0
B_1, nT 0.0
-2.0
2.0
B_2, nT 0.0
-2.0
2.0
B_3, nT 0.0
-2.0
2.0
IBI, nT 1.5
1.0
2315
2320
2325
2330
2335
2340
2345
Time, UT

(*a*)

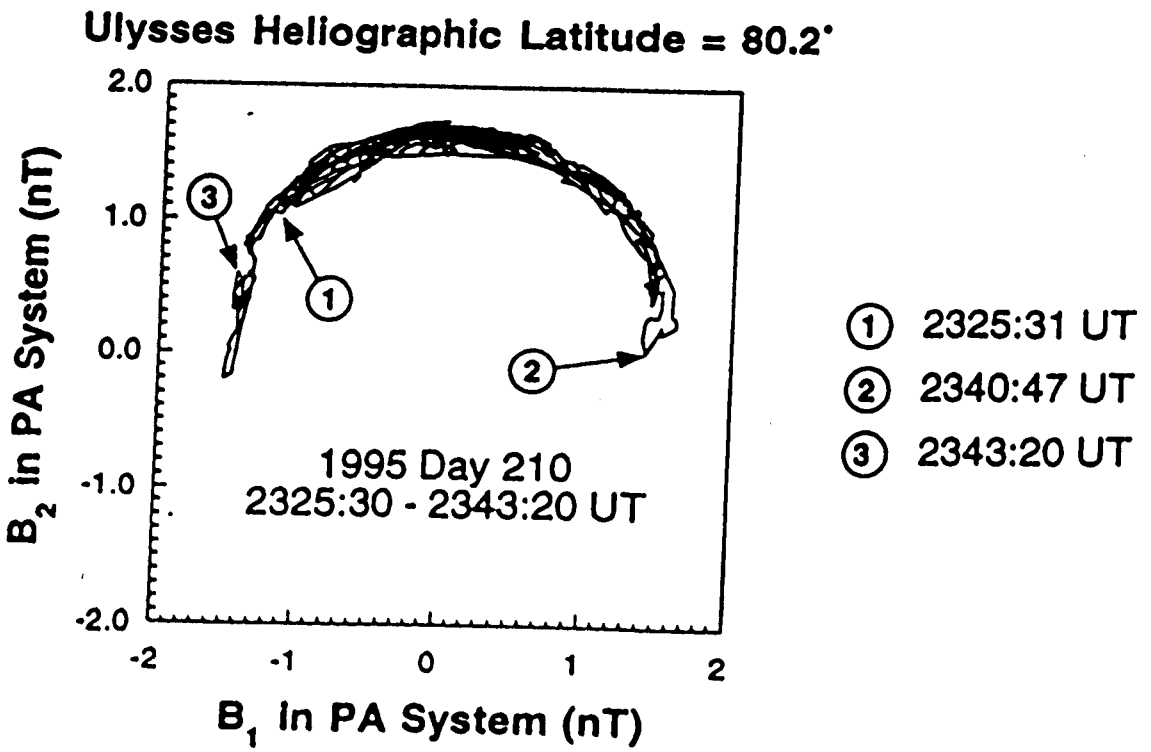
Ulysses Heliographic Latitude = 80.2°
2.0
1.0
0.0
-1.0
-2.0
B_2 in PA System (nT)
-2
-1
0
1
2
B_1 in PA System (nT)
1995 Day 210
2325:30 - 2343:20 UT
1 2325:31 UT
2 2340:47 UT
3 2343:20 UT

(*b*)

Fig 1D

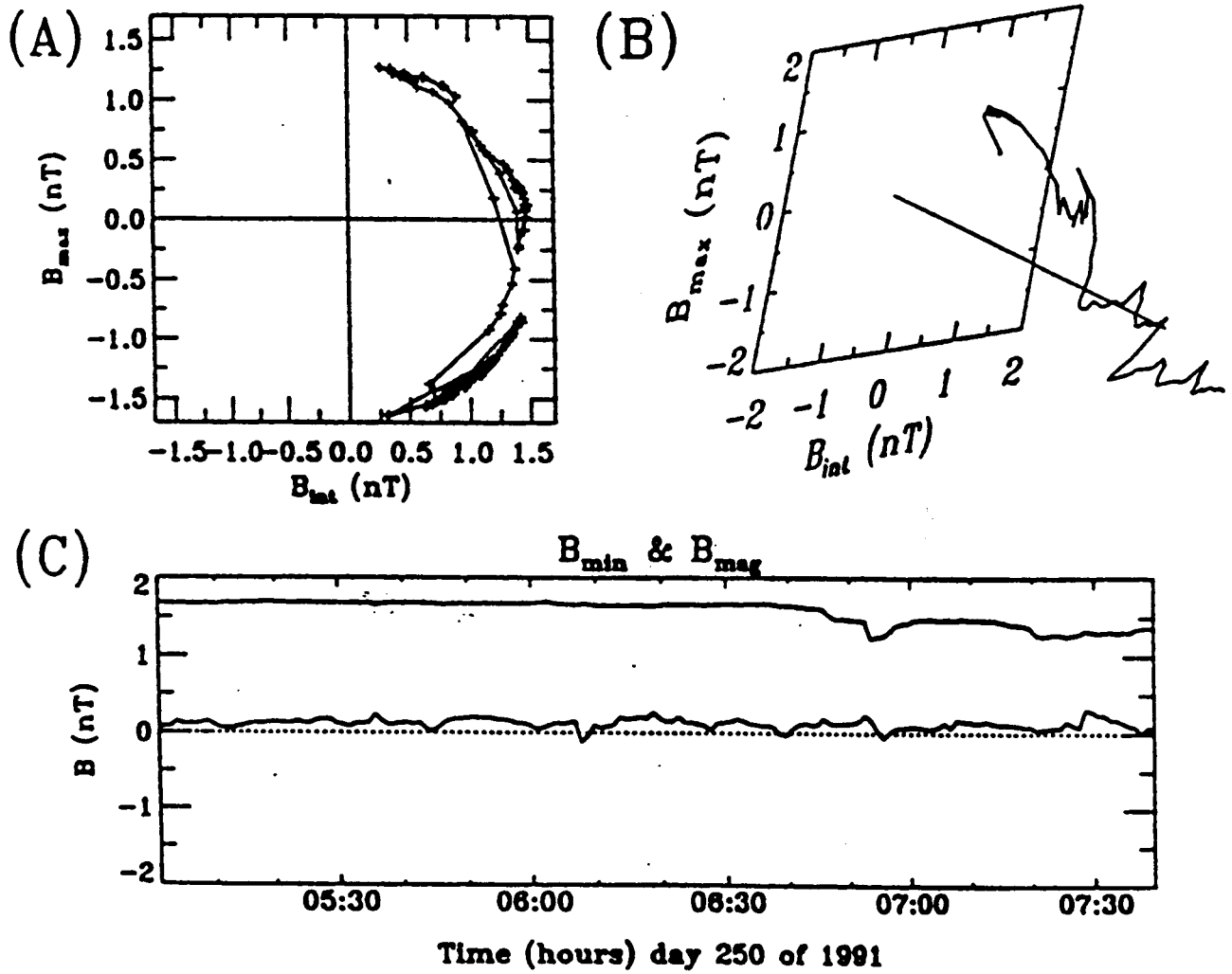
(A)
1.5
1.0
0.5
0.0
−0.5
−1.0
−1.5
B_{max} (nT)
−1.5 −1.0 −0.5 0.0 0.5 1.0 1.5
B_{int} (nT)
(B)
2
1
0
−1
−2
B_{max} (nT)
−2 −1 0 1 2
B_{int} (nT)
(C)
B_{min} & B_{mag}
2
1
0
−1
−2
B (nT)
05:30
06:00
06:30
07:00
07:30
Time (hours) day 250 of 1991

Fig 11

Planar Waves

Spherical Waves

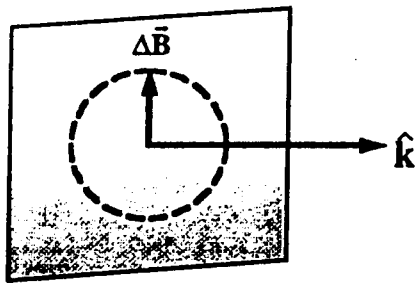

Circular Polarization

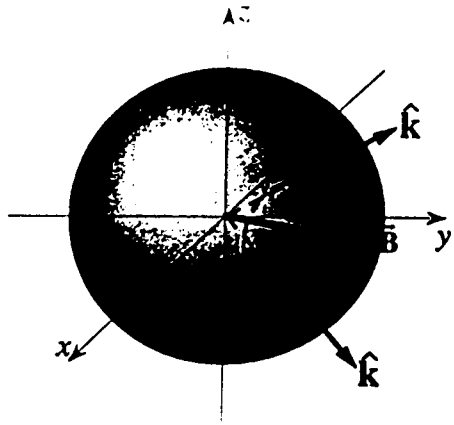

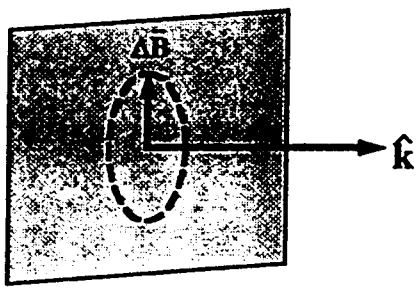

Elliptical Polarization

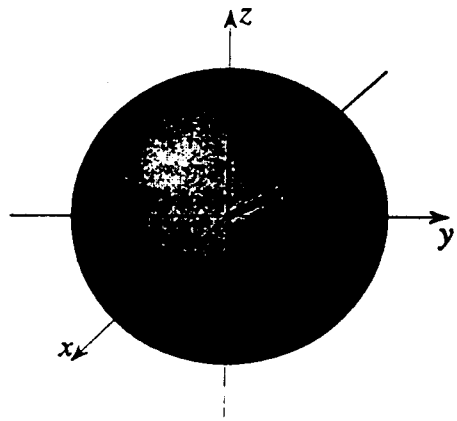

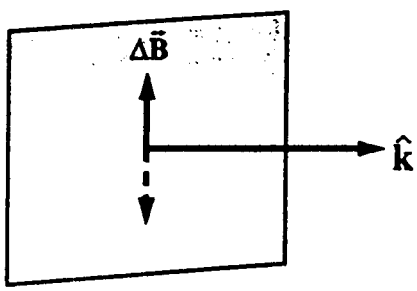

Linear/Arc Polarization

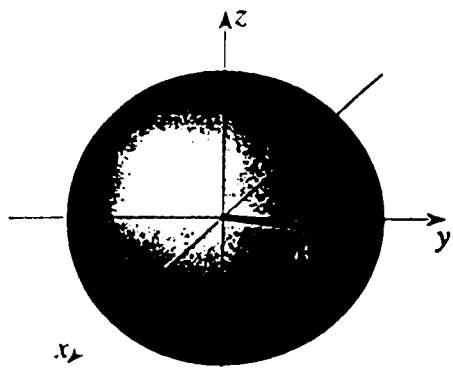

a)

b)

Fig 17

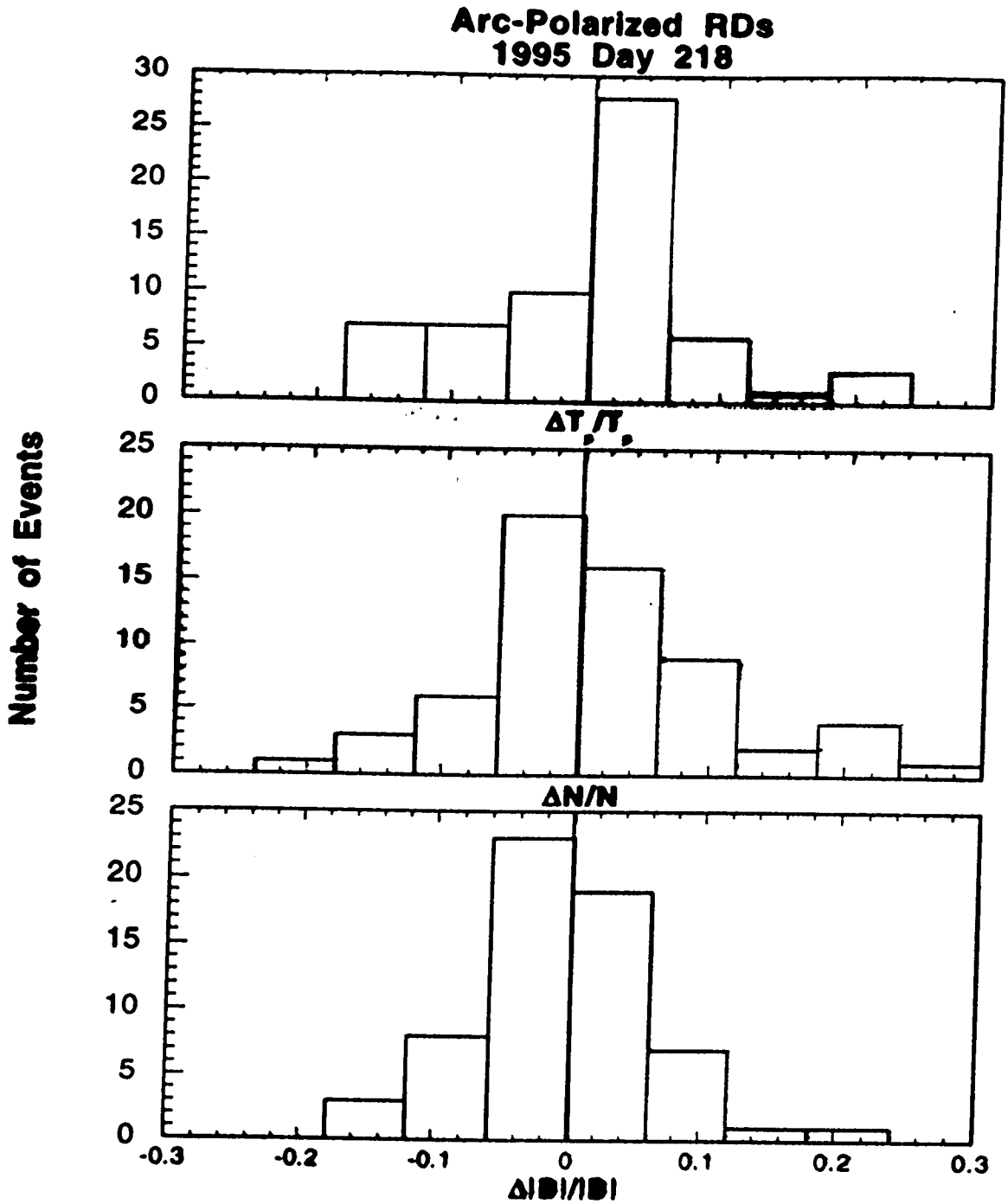
Arc-Polarized RDs
1995 Day 218
Number of Events
30
25
20
15
10
5
0
ΔT⊥/T⊥
25
20
15
10
5
0
ΔN/N
25
20
15
10
5
0
-0.3
-0.2
-0.1
0
0.1
0.2
0.3
Δ|B|/|B|

Fig 13

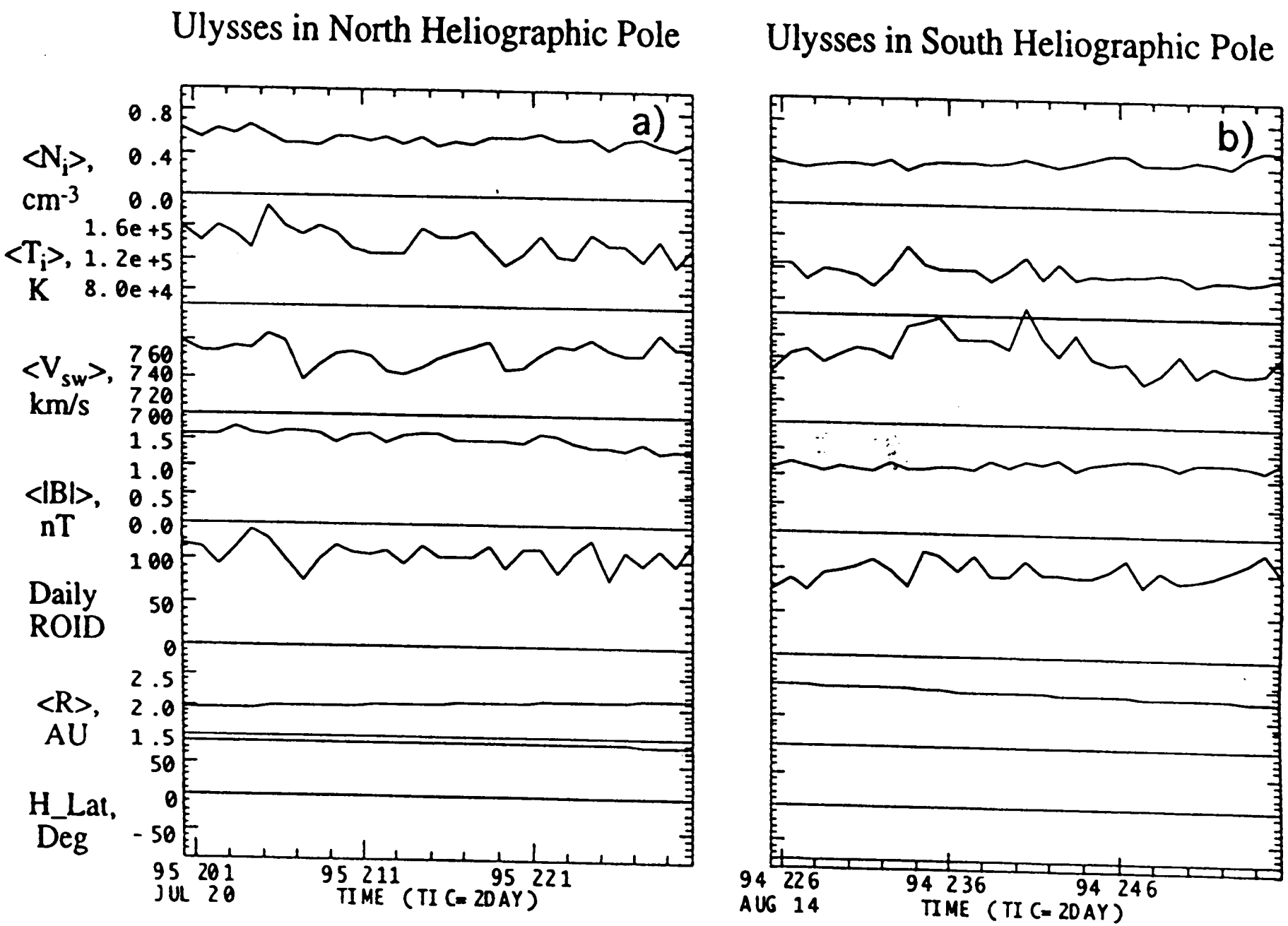
Ulysses in North Heliographic Pole
Ulysses in South Heliographic Pole
a)
b)
<N_i>, cm^-3
0.8
0.4
0.0
<T_i>, K
1.6e+5
1.2e+5
8.0e+4
<V_sw>, km/s
760
740
720
700
<|B|>, nT
1.5
1.0
0.5
0.0
Daily ROID
100
50
0
<R>, AU
2.5
2.0
1.5
H_Lat, Deg
50
0
-50
95 201
JUL 20
95 211
95 221
TIME (TIC=2DAY)
94 226
AUG 14
94 236
94 246
TIME (TIC=2DAY)

Fig 14

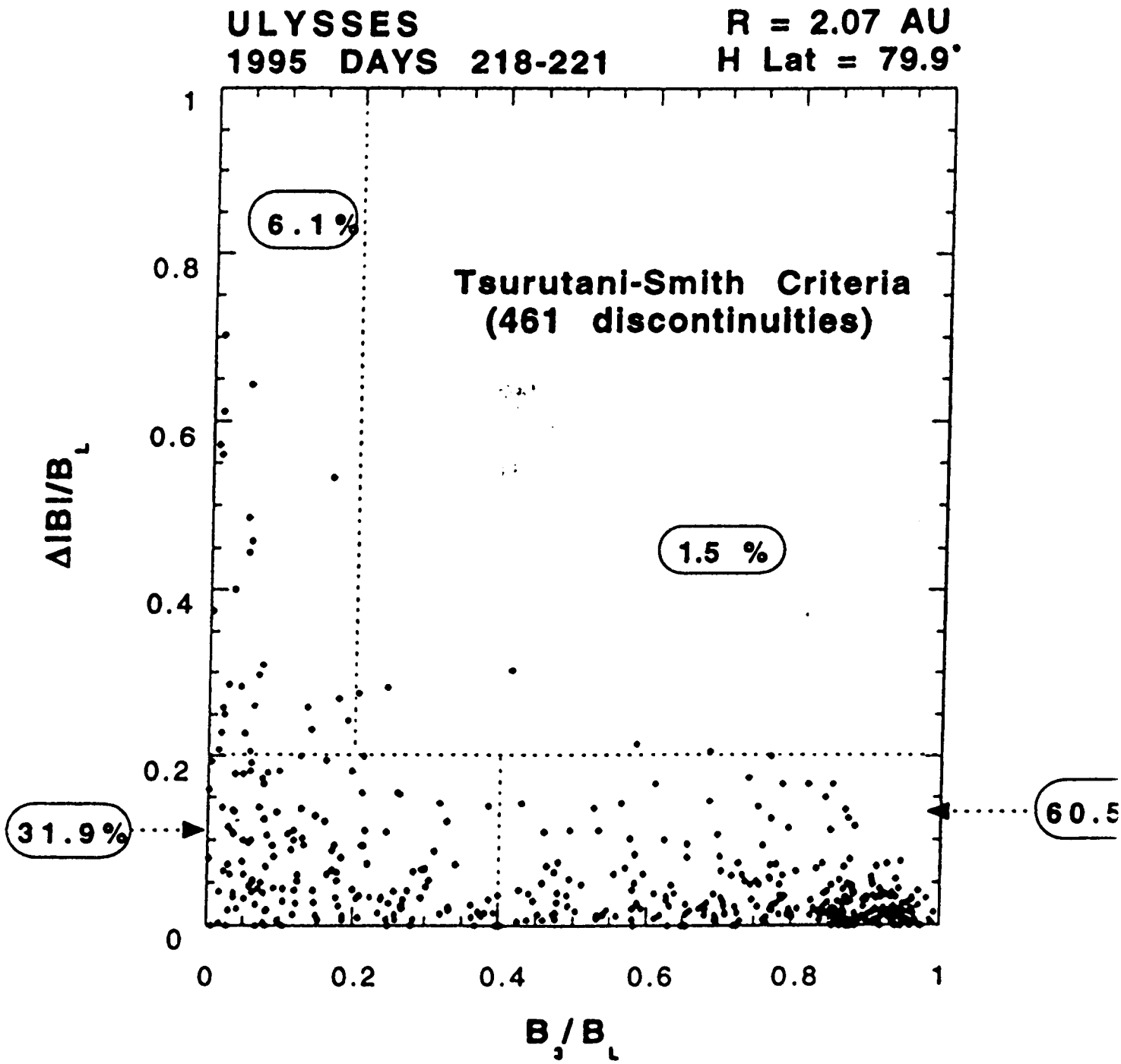
ULYSSES
1995 DAYS 218-221
R = 2.07 AU
H Lat = 79.9°
Tsurutani-Smith Criteria
(461 discontinuities)
6.1%
1.5 %
31.9%
60.5
ΔIBI/B_L
B_J/B_L
0
0.2
0.4
0.6
0.8
1

Fig 15

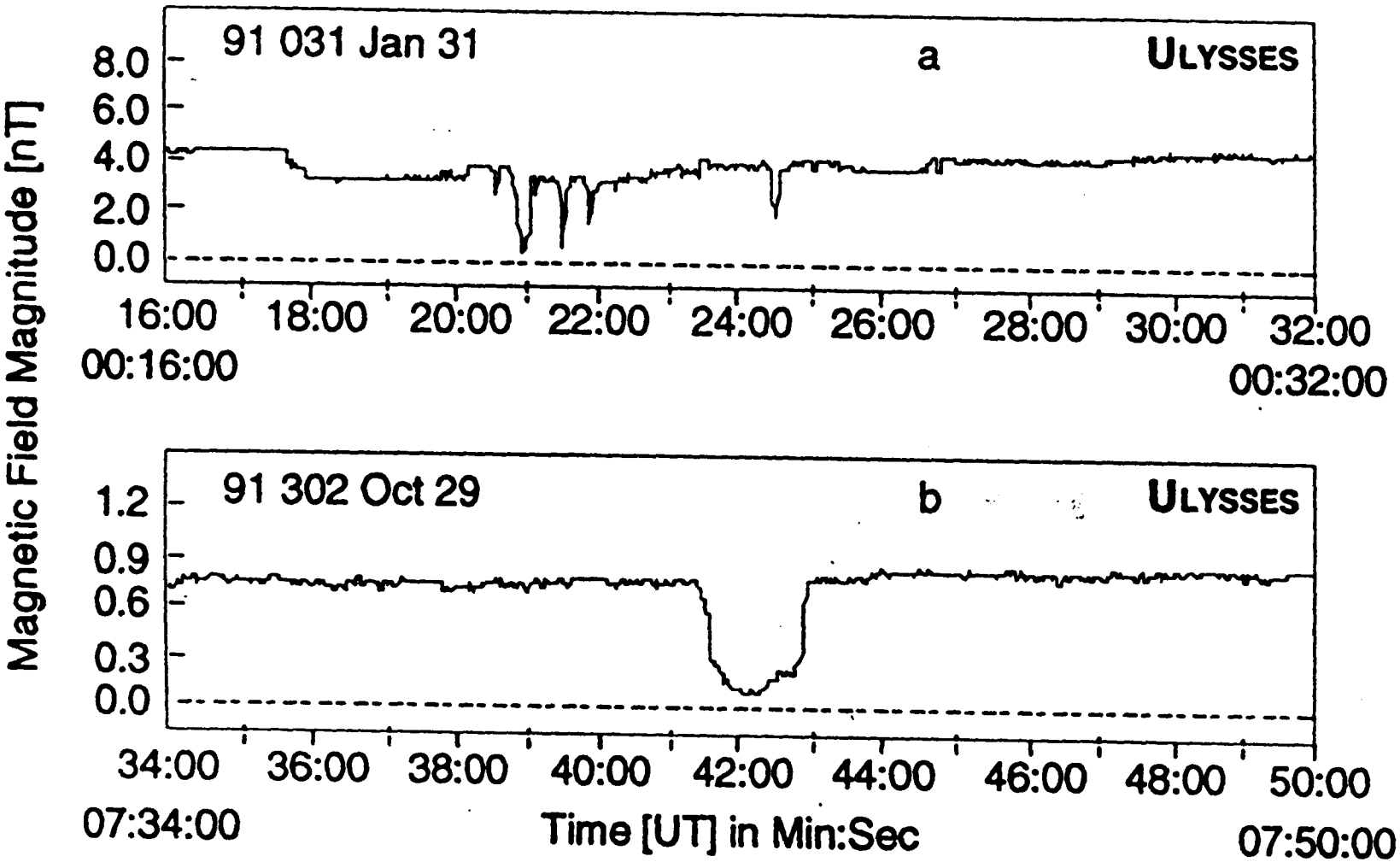
91 031 Jan 31
a
ULYSSES
8.0
6.0
4.0
2.0
0.0
16:00
18:00
20:00
22:00
24:00
26:00
28:00
30:00
32:00
00:16:00
00:32:00
91 302 Oct 29
b
ULYSSES
1.2
0.9
0.6
0.3
0.0
34:00
36:00
38:00
40:00
42:00
44:00
46:00
48:00
50:00
07:34:00
07:50:00
Magnetic Field Magnitude [nT]
Time [UT] in Min:Sec

Fig 16

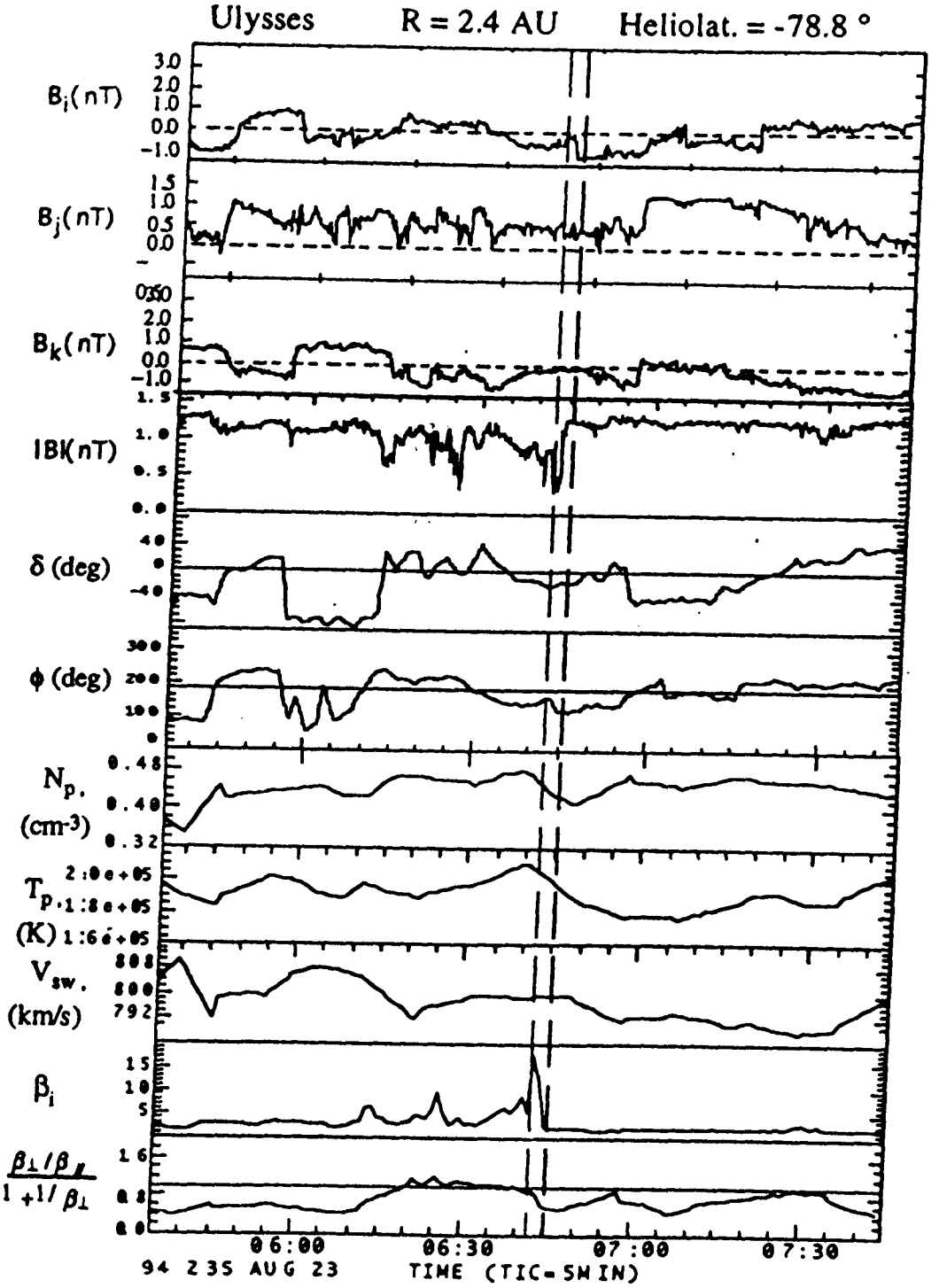
Ulysses R = 2.4 AU Heliolat. = -78.8 °
B_i(nT)
B_j(nT)
B_k(nT)
|B|(nT)
δ (deg)
φ (deg)
N_p, (cm^{-3})
T_p (K)
V_{sw}, (km/s)
β_i
$\frac{\beta_\perp / \beta_\parallel}{1 + 1/\beta_\perp}$
06:00
06:30
07:00
07:30
94 235 AUG 23
TIME (TIC=5MIN)

Fig 17

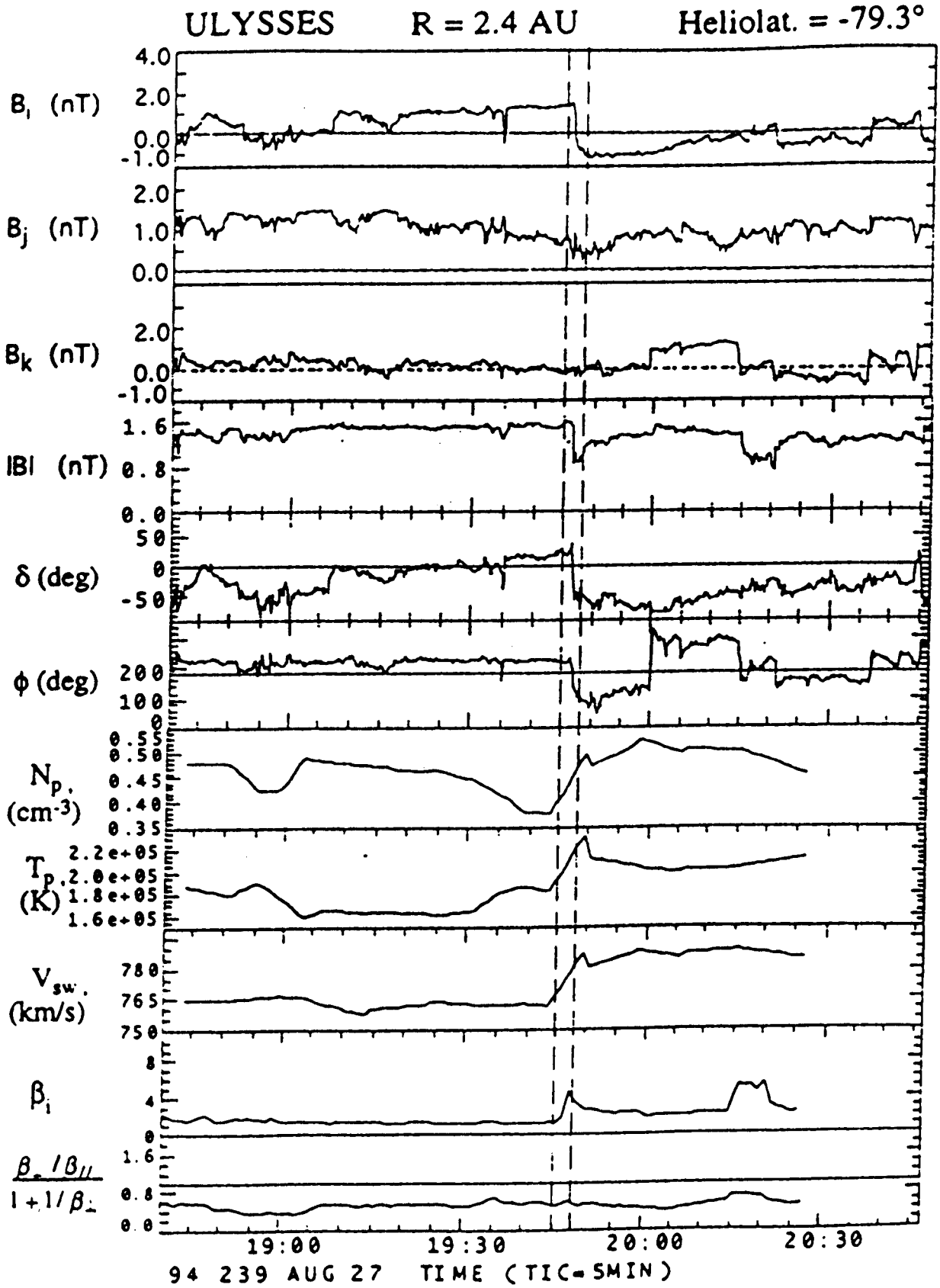
ULYSSES
R = 2.4 AU
Heliolat. = -79.3°
B_i (nT)
B_j (nT)
B_k (nT)
|B| (nT)
δ (deg)
φ (deg)
N_p, (cm^{-3})
T_p, (K)
V_{sw}, (km/s)
β_i
$\frac{\beta_\perp / \beta_\parallel}{1 + 1/\beta_\perp}$
19:00
19:30
20:00
20:30
94 239 AUG 27 TIME (TIC=5MIN)

Fig 18

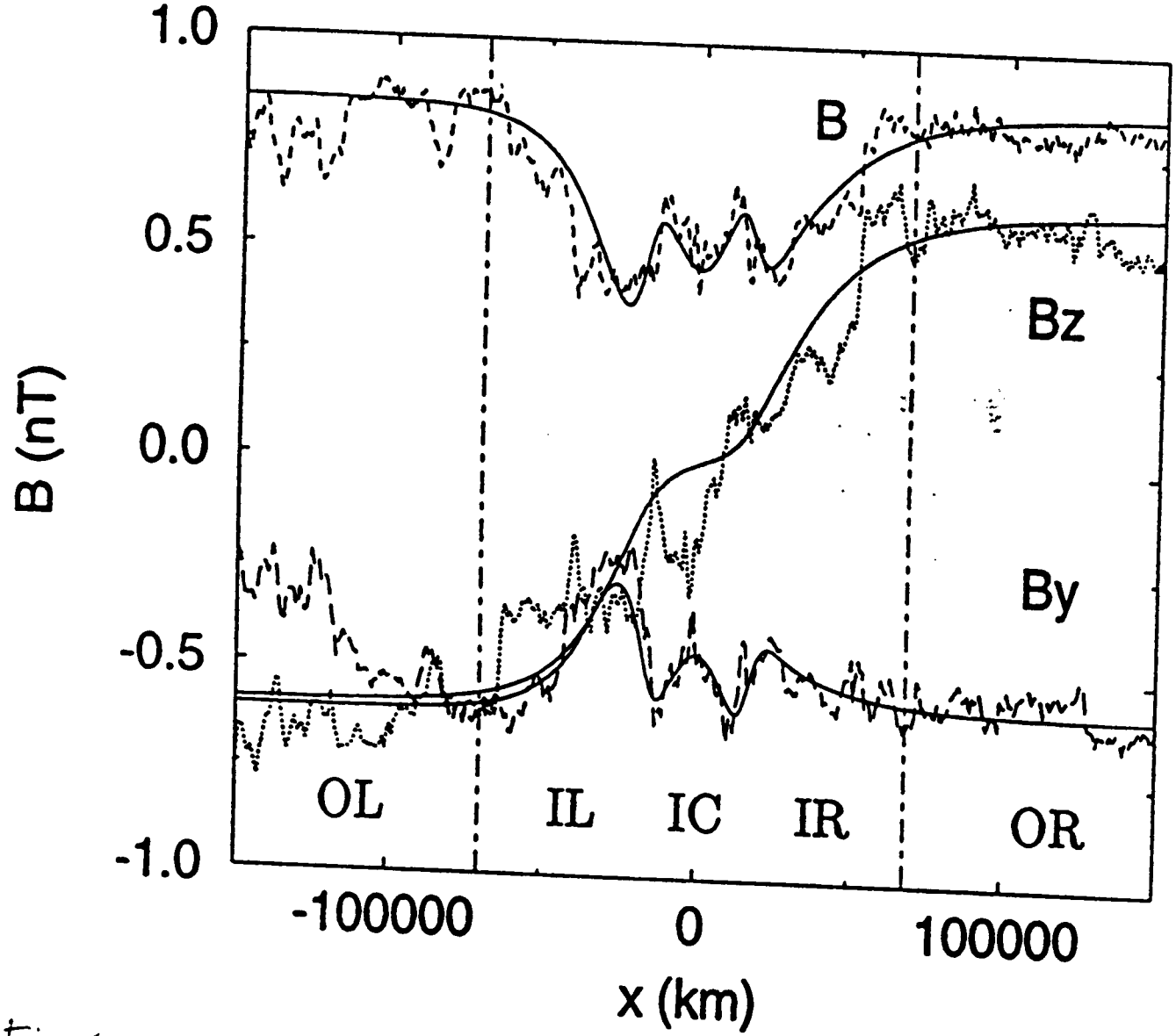

Fig 19

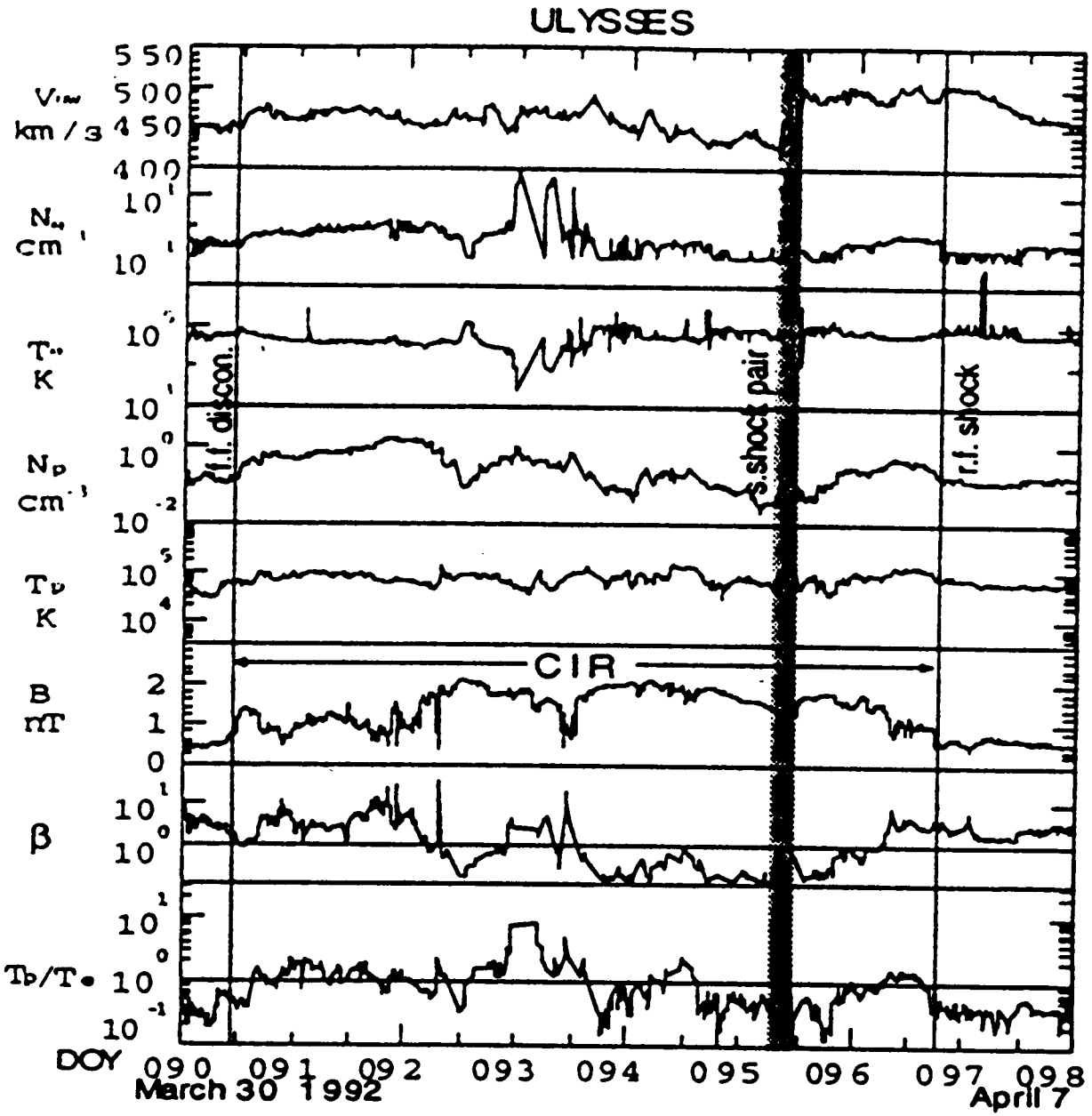
ULYSSES
550
500
450
400
V_{sw}
km / s
10^{1}
10^{0}
N_e
cm^{-3}
10^{5}
10^{4}
T_e
K
10^{1}
10^{0}
10^{-2}
N_p
cm^{-3}
10^{5}
10^{4}
T_p
K
CIR
2
1
0
B
nT
10^{1}
10^{0}
β
10^{1}
10^{0}
10^{-1}
T_p/T_e
r.f. discon.
S.shock pair
r.f. shock
DOY
090
091
092
093
094
095
096
097
098
March 30 1992
April 7

Fig 20

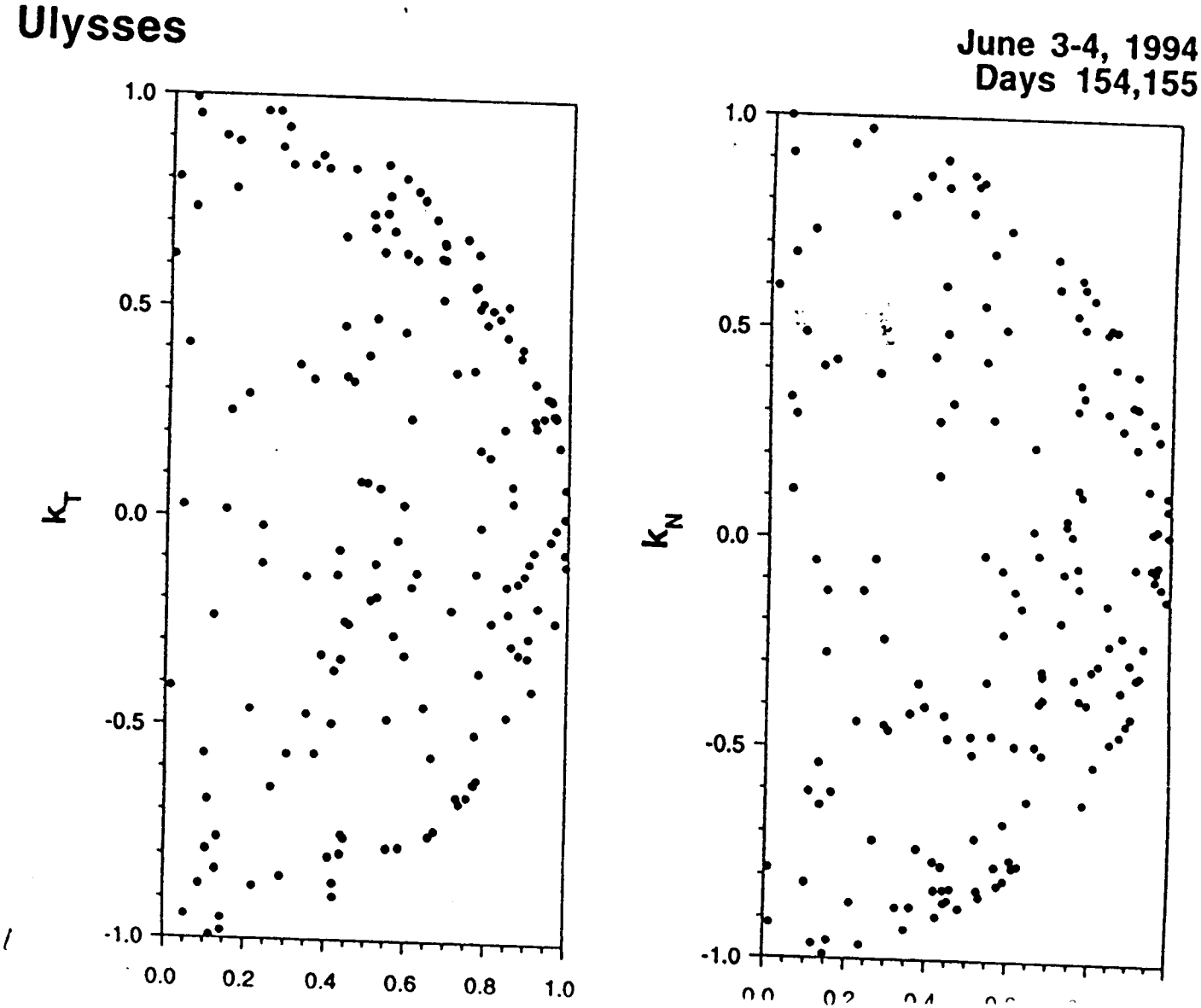
Ulysses
June 3-4, 1994
Days 154,155
k_T
k_N
1.0
0.5
0.0
-0.5
-1.0
0.0
0.2
0.4
0.6
0.8
1.0

Fig 21

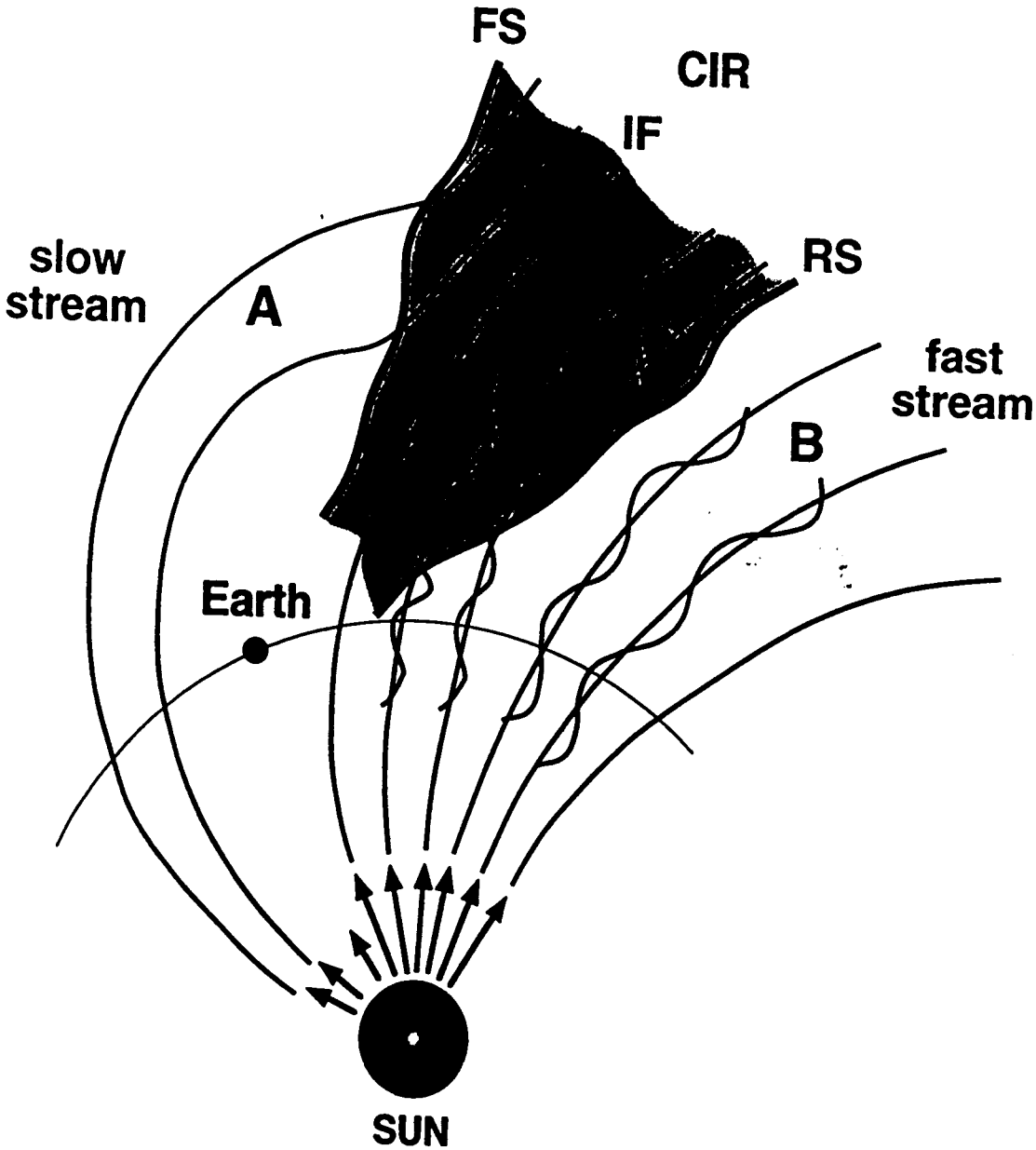

Fig 22

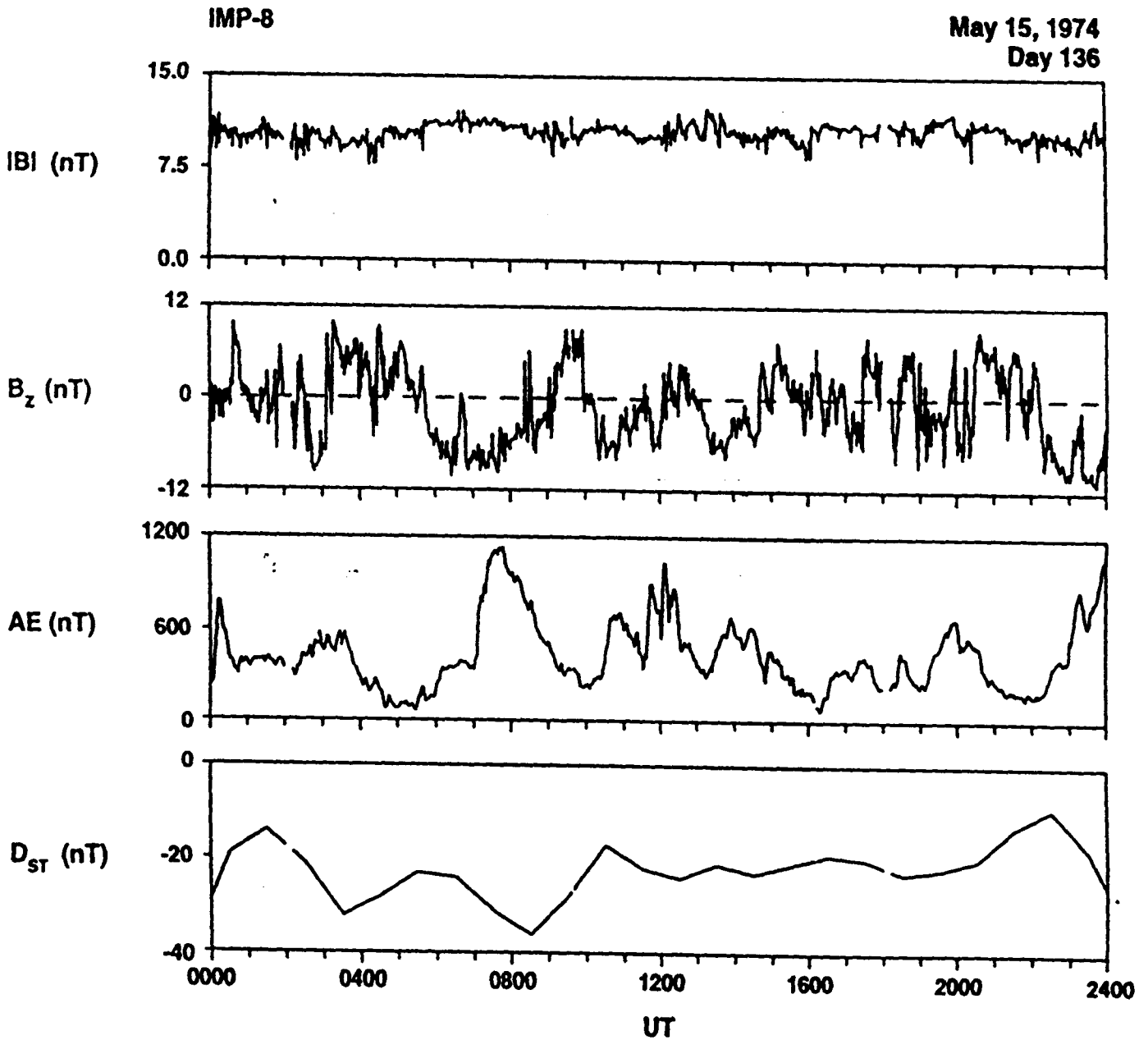
IMP-8
May 15, 1974
Day 136
15.0
7.5
0.0
|B| (nT)
12
0
-12
B_z (nT)
1200
600
0
AE (nT)
0
-20
-40
D_{ST} (nT)
0000
0400
0800
1200
1600
2000
2400
UT

Fig 23